Journal of Hydrology 570 (2019) 508–522

Contents lists available at ScienceDirect

Journal of Hydrology

journal homepage: www.elsevier.com/locate/jhydrol

Research papers

A framework to quantify impacts of elevated CO_2 concentration, global warming and leaf area changes on seasonal variations of water resources on a river basin scale

Wei Qi[a,b,c], Junguo Liu[a,b,c,*], Felix Leung[d]

[a] School of Environmental Science and Engineering, Southern University of Science and Technology, Shenzhen 518055, China
[b] Guangdong Provincial Key Laboratory of Soil and Groundwater Pollution Control, School of Environmental Science and Engineering, Southern University of Science and Technology, Shenzhen 518055, China
[c] State Environmental Protection Key Laboratory of Integrated Surface Water-Groundwater Pollution Control, School of Environmental Science and Engineering, Southern University of Science and Technology, Shenzhen 518055, China
[d] Institute of Environment, Energy and Sustainability, Chinese University of Hong Kong, Hong Kong

ARTICLE INFO

This manuscript was handled by Emmanouil Anagnostou, Editor-in-Chief

Keywords:
CO_2
Warming
Vegetation changes
Runoff
Water resources

ABSTRACT

With concerns about future catastrophic disasters, elevated CO_2 concentration (eCO_2), global warming and vegetation changes have received much attention globally. In recent years, studies have suggested controlling climate change should be based on regional impacts. However, regional quantitative assessments of respective and combination influences of CO_2, temperature and vegetation variations on water resources remain limited. To address this issue, a comprehensive framework is developed. This framework integrates a dynamic vegetation simulation approach, a biosphere hydrological model and a variance-based sensitivity analysis approach which enables identification of predominant influential factors including their combinations. A medium-sized river basin in northeast China is used to illustrate the application based on different CO_2 concentration and temperature rise assumptions. Validation using MODIS products shows the proposed approach can simulate Leaf Area Index (LAI) changes well. Results show sum of the influences of LAI and temperature variations on transpiration are more than 1.6 times higher than physiological effects of eCO_2 in growing seasons, which implies more water could be transpired than conserved with eCO_2, global warming and LAI changes. Results also show runoff increases with eCO_2 and decreases with increasing temperatures, but LAI changes play a dominate role in runoff decrease in hot summer. Therefore, considering LAI changes is of utmost importance in projections of future water resources, and severity of future water shortage could be underestimated if LAI changes are neglected. This research is useful in gaining insights into the complicated impacts of eCO_2, global warming and LAI changes on regional water security and sustainability.

1. Introduction

It has been reported that global average temperature is rising with elevated CO_2 concentration (Hansen et al., 2012; Fischer et al., 2013). With CO_2 concentration and temperature variations, global vegetation changes have also been reported in some regions (Piao et al., 2007; Hansen et al., 2013; Zhu et al., 2016). These changes have caused worries that they could result in catastrophic disasters, for example, severe droughts and water scarcity (Seager et al., 2007; Dai, 2013; Fischer et al., 2013; Jaeger et al., 2014; Hu et al., 2015; Irvine et al., 2017; Baker et al., 2018).

To ameliorate the negative influences of the changes in CO_2 concentration, temperature and vegetation, Seneviratne et al. (2016) suggested that CO_2 emissions should be limited based on regional climate change impacts because regional impacts are more directly related to individual interests and global average temperature targets may fail to represent the urgency of controlling climate change. Similarly, many recent studies also suggested that climate change limitation should be based on its impacts on regional scales (e.g., Matthews et al., 2017, Seneviratne et al., 2018, Greve et al., 2018). Therefore, regional studies of the influences of elevated CO_2 concentration, temperature variations and vegetation dynamics on water resources are imperative and

* Corresponding author at: School of Environmental Science and Engineering, Southern University of Science and Technology, Shenzhen 518055, China.
E-mail address: liujg@sustc.edu.cn (J. Liu).

https://doi.org/10.1016/j.jhydrol.2019.01.015
Received 24 September 2018; Received in revised form 2 January 2019; Accepted 7 January 2019
Available online 19 January 2019
0022-1694/

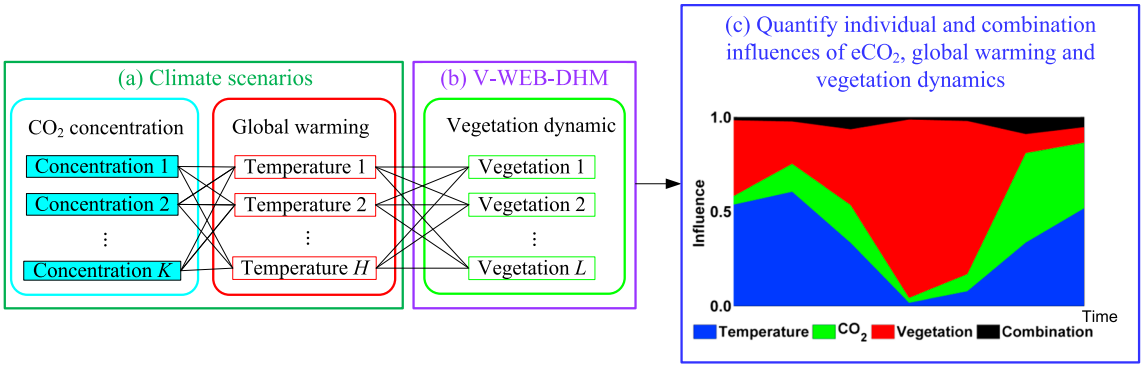

Fig. 1. Schematic diagram of the developed framework to factorize the respective and combination influences of elevated CO_2 concentration (eCO_2), global warming and vegetation dynamics on simulated land surface fluxes and hydrological variables. *K* CO_2 concentration scenarios, *H* temperature rise scenarios and *L* vegetation dynamic scenarios are used to represent the changes.

essential.

Temperature, CO_2 and vegetation changes could influence water cycle in a very complex way. Increasing CO_2 concentration could warm the Earth, and variations in CO_2 concentration and/or temperature then may lead to changes in vegetation. At the leaf level, higher CO_2 concentration may lead to decrease in leaf stomatal conductance and therefore reduce transpiration rate (Field et al., 1995; Skinner et al., 2018). At the canopy level, CO_2 may increase Leaf Area Index (LAI) (Piao et al., 2007; Donohue et al., 2013, 2017; Zhu et al., 2016) and boost canopy transpiration and vegetation water use in soil (Pu and Dickinson, 2012; Swann et al., 2016; Zhang et al., 2016; Trancoso et al., 2017).

Many studies have investigated the impacts of CO_2 concentration, temperature and/or vegetation changes on water resources on global or continental scales (e.g., Labat et al., 2004; Gedney et al., 2006; Betts et al., 2007). Piao et al. (2007) concluded mean climate and its variability contribute to global runoff increase. Gerten et al. (2008) confirmed the research by Piao et al. (2007), and suggested that quantifying relative contributions of each individual contributors, such as CO_2 concentration, temperature and vegetation changes, to runoff variations are important and need to be carried out. Many recent studies have endeavoured to quantify the influences of CO_2 concentration, temperature and/or vegetation changes on a river basin scale, for example, the studies by Cheng et al. (2014) in Australia, Tao et al. (2014) in the Mississippi river basin and Tesemma et al. (2015) in the Murray-Darling river basin. Nevertheless, these studies on river basins did not separate the relative and combination influences of CO_2 concentration, temperature and vegetation changes on water resources variations. Consequently, studies that quantify the respective and combination influences remain limited on river basin scales. To quantify the influences on river basin scales, a comprehensive model is required, in which vegetation changes, photosynthesis-conductance variations and biosphere hydrological processes can be simulated simultaneously.

Sensitivity analysis is a useful approach to attribute changes to various influential factors (Wilby and Harris, 2006; Steinschneider et al., 2012; Wu et al., 2012a,b; Bosshard et al., 2013). In recent years, several studies have been carried out to investigate impacts of individual influential factors and their combinations on model simulation results based on advanced sensitivity analysis approaches. For example, Qi et al. (2016a) investigated impacts of precipitation data and hydrological models on runoff simulation uncertainty; Qi et al. (2016c) studied impacts of probability distribution functions, distribution function parameters and flood data on design flood selections. In these studies, an advanced variance-based sensitivity analysis approach (ANOVA) (Bosshard et al., 2013) was used because it allows for identification of predominant influential factors including their combinations, and provides a more complete understanding of the influential factors in a modelling chain.

The overall objective of this study is to develop a comprehensive framework to quantify the respective and combination influences of increasing CO_2 concentration, temperature variations and vegetation changes on water resources on a river basin scale. For this objective, a regional dynamic vegetation simulation approach is developed and incorporated into the WEB-DHM model (V-WEB-DHM) first, and then the comprehensive framework is proposed by integrating V-WEB-DHM and ANOVA (described in Section 2). To illustrate the application of the developed framework, a medium-sized river basin in northeast China is used (introduced in Section 3), and the water resources variations on a multi-year mean monthly scale are investigated based on simulated vegetation changes and different CO_2 concentration and temperature rise assumptions (presented in Section 4). In this illustrative application, the vegetation dynamics/changes will refer to LAI changes and CO_2 influences will refer to the physiological effects of CO_2 concentration hereafter. This research is useful in gaining insights into the complicated impacts of increasing CO_2 concentration, temperature variations and leaf area changes on regional water resources and therefore on regional water security and water sustainability (provided in Sections 5 and 6).

2. The methods

The developed framework includes three components: (i) set up climate change scenarios, e.g., CO_2 concentration and temperature; (ii) under these climate conditions, calculate vegetation changes and simulate land surface fluxes and hydrological variables using V-WEB-DHM; and (iii) quantify the individual and combination influences of CO_2 concentration, temperature and vegetation changes on simulated results using ANOVA. Fig. 1 shows the diagrammatic representation of the developed framework. The details are introduced in the following sub-sections.

2.1. Structure of V-WEB-DHM

Fig. 2 shows overall structure of V-WEB-DHM. Fig. 2(a)–(d) represents the structure of WEB-DHM; Fig. 2(e) shows vegetation dynamics which are results of many environmental resources, such as precipitation, solar radiation, temperature, CO_2, humidity and wind speed.

In Fig. 2(d), canopy conductance g_c is simulated by combining a leaf stomatal conductance model developed by Ball (1988) and a photosynthesis model developed by Collatz et al. (1991, 1992) (i.e., the Ball-Berry model)

$$g_c = m \cdot \frac{A_c}{C_s} \cdot Rh \cdot p + b \cdot \mathrm{LAI} \quad (1)$$

where m and b are coefficients (Sellers et al., 1996a); Rh represents

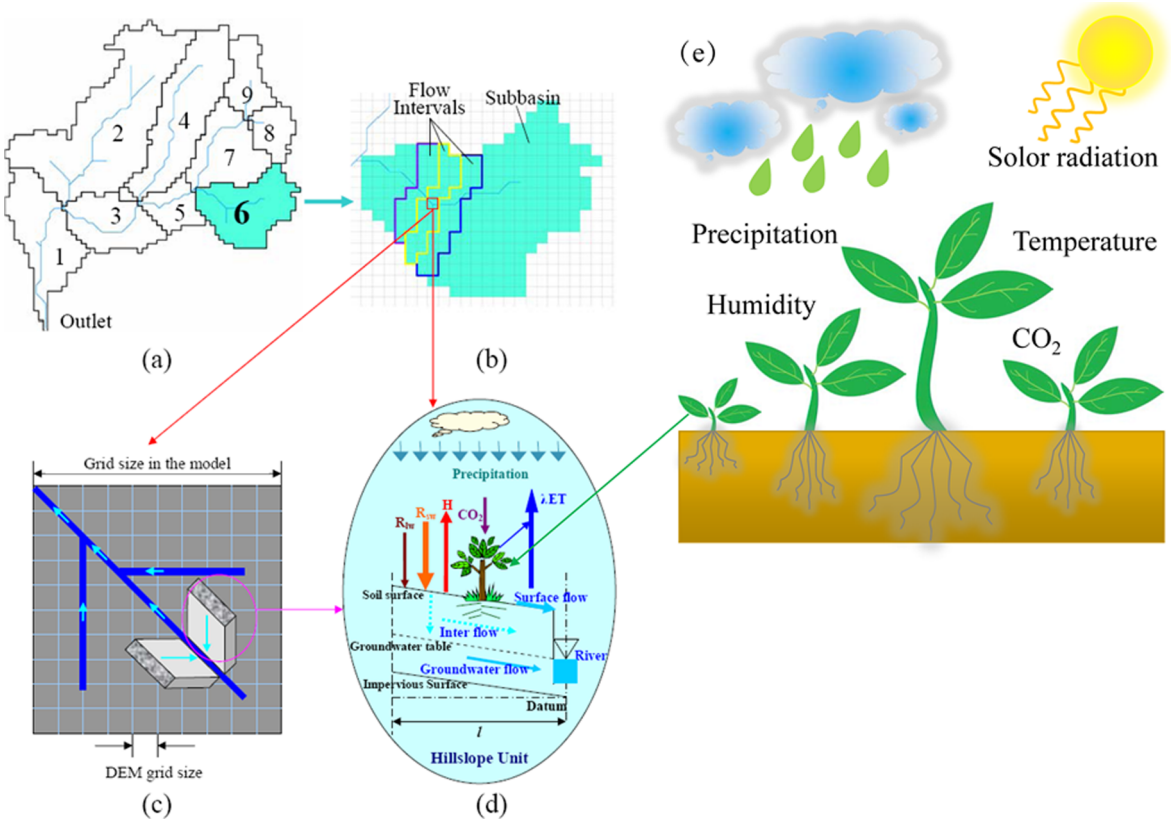

Fig. 2. Overall structure of V-WEB-DHM. (a) describes sub-basins; (b) illustrates subdivision from a sub-basin to flow intervals comprising several model grids; (c) explains discretization from a model grid to a number of geometrically symmetrical hillslopes; (d) details process descriptions of water moisture transfer from atmosphere to river, including downward solar radiation (R_{sw}), downward long wave radiation (R_{lw}), sensible heat flux (H) and latent heat of vaporization (λET); (e) represents vegetation dynamics. (a) – (d) are on the basis of the research by Wang et al. (2009).

relative humidity; C_s represents CO_2 partial pressure (Pa); P represents atmospheric pressure (Pa); A_c represents a canopy photosynthetic rate. The photosynthetic rate is calculated as the minimum of three limiting rates. For C3 species, they are efficiency of photosynthetic enzyme system, incident radiation absorbed by green canopy and the capacity of leaf to utilize or export the products of photosynthesis; for C4 species, they are Rubisco limitation, light limitation and PEP-Carboxylase limitation (Collatz et al., 1992; Sellers et al., 1996a). The canopy conductance rate is then used to estimate canopy transpiration rate E_{ct}

$$E_{ct} = \left[\frac{e(T_c) - e_a}{1/g_c + 2\cdot r_b}\right]\cdot\frac{\rho\cdot c_p}{\gamma}\cdot(1 - W_c) \tag{2}$$

where $e(T_c)$ represents saturated vapour pressure (Pa) when canopy temperatures equal T_c; e_a represents vapour pressure (Pa); ρ and c_p are density and specific heat of air; γ represents the psychrometric constant; W_c represents canopy wetted area. Based on Eqs. (1) and (2), it can be seen that the canopy transpiration and stomatal conductance are influenced by many environmental variables, such as LAI, CO_2 concentration, relative humidity and temperature. More details about the calculations of g_c and E_{ct} can be found in the research by Sellers et al. (1996a). Land use types are defined based on biomes, and are the same to the classifications in the Simple Biosphere model version 2 (SiB2) (Randall et al., 1996; Sellers et al., 1996b). The different responses of biomes to CO_2 concentration changes are represented by biome dependent parameters through lookup tables. The lookup tables used in this study are the same to the studies by Sellers et al. (1996b) and Randall et al. (1996). More detailed descriptions about WEB-DHM can be found in the studies by Wang et al. (2009), Qi et al. (2015, 2018a).

2.2. LAI simulation approach

LAI refers to one-sided leaf areas per unit ground. LAI represents mass accumulation in plant leaves, and is a result of vegetation growth influenced by availability of water, light, temperature, CO_2 and humidity, etc (Yang et al., 2016; Donohue et al., 2017). LAI can be simulated based on these environmental resources. For example, Jamieson et al. (1998) developed an approach to simulate LAI based on an exponential function and temperature. Similarly, Koetz et al. (2005) and Setiyono et al. (2008) developed approaches based on an exponential function and temperature as well. In addition, Cao et al. (2015) and Su et al. (2015) proposed a LAI simulation approach based on an exponential distribution using accumulated growing degree days; Tesemma et al. (2015) developed a method based on precipitation, potential evapotranspiration and an exponential function. In these prior studies, temperature, precipitation and potential evapotranspiration were considered to simulate LAI. However, LAI has different responses to climate in different regions (Zhu et al., 2016). Thus, it is necessary to develop a simple and general approach to simulate LAI dynamics.

Different from previous research, in this study, a LAI simulation approach is developed based on SiB2 biome types and corresponding biome dependent morphological properties in SiB2 lookup tables (please refer to the study by Randall et al. (1996) for the biome types on a global scale). In this new approach, all environmental resources (i.e., precipitation, temperature, solar radiation, long wave radiation, humidity, CO_2, etc.) that strongly related to LAI variations can be taken into consideration. The developed LAI simulation approach is as below:

$$\mathrm{LAI} = \frac{x_{n+2}\cdot \mathrm{LAI}_{\max}}{1 + \exp[x_{n+1} - (x_1\cdot V_1 + x_2\cdot V_2 + \cdots + x_{n-1}\cdot V_{n-1} + x_n\cdot V_n)]} \tag{3}$$

where LAI represents simulated values; $\mathrm{LAI}_{\max}$ represents the maximum

LAI values of each SiB2 vegetation type, and is obtained from SiB2 database; $(V_1, V_2, \cdots, V_{n-1}, V_n)$ represent environmental variables influencing vegetation growth, such as precipitation, temperature, light, CO_2 and humidity; $(x_1, x_2, \cdots, x_{n-1}, x_n)$ represent influences of each environmental resource on LAI; x_{n+1} represents the states without environmental resource influence; x_{n+2} represents changes of local maximum LAI values relative to the maximum LAI values in SiB2 database; 'exp' represents an exponential function. In practical application, $(x_1, x_2, \cdots, x_{n-1}, x_n, x_{n+1}, x_{n+2})$ should be quantified based on experience, experiments and/or calibrations.

In the last few decades, the quick development of remote sensing techniques provides a great number of datasets about vegetation dynamics, which enable very detailed, reliable and quantitative analyses of spatial and temporal variations of LAI. Thus, the parameters in Eq. (3) can be derived from these remote sensing data sets. One approach is to calibrate with an objective function using auto-calibration algorithms, such as the Dynamically Dimensioned Search (DDS) algorithm (Tolson and Shoemaker, 2007), the shuffled complex evolution approach (Duan et al., 1993; Qi et al., 2016b) and the non-dominated sorting genetic algorithm II (Deb and Gupta, 2006; Qi et al., 2018c).

2.3. Anova

Ensemble simulation results can be obtained using V-WEB-DHM with different CO_2 concentration, air temperature rises and vegetation conditions as inputs. Total ensemble width M is the variance of simulated land surface and hydrological variables. To relate M to influential sources, the superscripts j, k and l in $M^{j,k,l}$ are used to represent temperature scenario j, CO_2 concentration scenario k and vegetation scenario l.

ANOVA can underestimate variance when a small sample size is utilized (Bosshard et al., 2013). To reduce the bias effects on variance contribution quantification, a subsampling method proposed by Bosshard et al. (2013) is used in this study. This subsampling method randomly selects two samples from the largest sample set (assume to be H) without replacement and generates a new sample set to be used for ANOVA. With this subsampling, the superscript j in $M^{j,k,l}$ is replaced with $\mathbf{g}(h, i)$, which is a $2 \times C_2^H$ matrix as follows

$$\mathbf{g} = \begin{pmatrix} 11\cdots 1 & 22\cdots H-3 & H-3 & H-3 & H-2 & H-2 & H-1 \\ 23\cdots H & 34\cdots H-2 & H-1 & H & H-1 & H & H \end{pmatrix} \quad (4)$$

Total sum of squares (SST) can be divided into sums of squares of individual and combination effects:

$$\mathrm{SST} = \mathrm{SSA} + \mathrm{SSB} + \mathrm{SSC} + \mathrm{SSI} \quad (5)$$

where SSA represents influence of CO_2 concentration changes; SSB represents influence of temperature changes; SSC represents influence of vegetation changes; SSI represents influence of their combinations.

The terms can be estimated as follows (SSI is computed as the residual) (Bosshard et al., 2013):

$$\mathrm{SST_i} = \sum_{\mathrm{h=1}}^{\mathrm{H}} \sum_{\mathrm{k=1}}^{\mathrm{K}} \sum_{\mathrm{l=1}}^{\mathrm{L}} (\mathrm{M^{g(h,i),k,l}} - \mathrm{M^{g(-,i),-,-}})^2 \quad (6)$$

$$\mathrm{SSA}_i = K \cdot L \cdot \sum_{h=1}^{H} (M^{g(h,i),-,-} - M^{g(-,i),-,-})^2 \quad (7)$$

$$\mathrm{SSB_i} = \mathrm{H \cdot L \cdot} \sum_{\mathrm{k=1}}^{\mathrm{K}} (\mathrm{M^{g(-,i),k,-}} - \mathrm{M^{g(-,i),-,-}})^2 \quad (8)$$

$$\mathrm{SSC_i} = \mathrm{H \cdot K \cdot} \sum_{\mathrm{l=1}}^{\mathrm{L}} (\mathrm{M^{g(-,i),-,l}} - \mathrm{M^{g(-,i),-,-}})^2 \quad (9)$$

$$\mathrm{SSI}_i = \sum_{h=1}^{H} \sum_{k=1}^{K} \sum_{l=1}^{L} (M^{g(h,i),k,l} - M^{g(h,i),-,-} - M^{g(-,i),k,-} - M^{g(-,i),-,l} + 2 \cdot M^{g(-,i),-,-})^2 \quad (10)$$

where symbol '–' indicates average values over a particular index. H, K and L are scenario sampling numbers of air temperature, CO_2 concentration and vegetation conditions. The individual influences of CO_2 concentration, temperature and vegetation changes and their combination influence can be calculated as follows:

$$\eta^2_{\mathrm{temperature}} = \frac{1}{I} \sum_{i=1}^{I} \frac{\mathrm{SSA}_i}{\mathrm{SST}_i} \quad (11)$$

$$\eta^2_{\mathrm{CO_2}} = \frac{1}{I} \sum_{i=1}^{I} \frac{\mathrm{SSB}_i}{\mathrm{SST}_i} \quad (12)$$

$$\eta^2_{\mathrm{Vegetation}} = \frac{1}{I} \sum_{i=1}^{I} \frac{\mathrm{SSC}_i}{\mathrm{SST}_i} \quad (13)$$

$$\eta^2_{\mathrm{Combination}} = \frac{1}{I} \sum_{i=1}^{I} \frac{\mathrm{SSI}_i}{\mathrm{SST}_i} \quad (14)$$

where $\eta^2_{\mathrm{temperature}}$, $\eta^2_{\mathrm{CO_2}}$, $\eta^2_{\mathrm{Vegetation}}$ and $\eta^2_{\mathrm{Combination}}$ have values between 0 and 1, and represent the relative influences of changes of temperature, CO_2 concentration, vegetation and their combinations. The higher the values, the larger the influences. As shown in Eqs. (11)–(14), the subsampling approach is necessary because it guarantees that every influential factor has the same denominator I, which ensures inter-comparisons among the influences are not affected by their different sampling numbers. The influence quantification using ANOVA takes all sources together, and does not repeat ANOVA for each influential factor. The combination effect represents influence from simultaneous variations of all the three factors, and reflects the influence of nonlinearity or interactions. In addition, observed runoff values or simulated variables using observed data are used to calculate the variance (see Bosshard et al. (2013) in which the used ANOVA approach is developed). Therefore, differences in the mean values of the three groups have no influence on the contribution quantification (Bosshard et al., 2013).

3. Study region, data materials and criteria for evaluation

3.1. The Biliu river basin

As one of the most populated areas in China, northeast China plays an important role in food production for supporting the livelihood of the population. This region frequently suffers from droughts which pose a threat to regional sustainable development. Thus, this study is conducted in a river basin, the Biliu river basin (2814 km^2) (Fig. 3), in northeast China. In addition, the Biliu river basin plays a very important role in water supply to nearby big cities, such as the Dalian city which has a population of 6.69 million, and the cities suffered from serious water shortages in recent years. The Dalian city government invested 660 million $ to tackle the water resources problem since 2008. Therefore, studies in the Biliu river basin on the water resources under climate change are both economically, environmentally and socially important.

3.2. Observation-based data

The data used in this study were collected from eleven rain gauges, one hydrology station and three meteorological gauges, from March 2000 to December 2010. Other data are also utilized including Digital Elevation Model (DEM) (Rabus et al., 2003) (Fig. 4a), USGS landuse types (Sellers et al., 1996a) (Fig. 4b), MOD15A2 one-km eight-day LAI and Fraction of Photosynthetically Active Radiation (FPAR) products (Myneni et al., 1997). There are six landuse types, with broadleaf and needleleaf trees, short vegetation/C4 grassland and agriculture/C3 grassland being the main types (Fig. 4b). Hourly precipitation data are obtained by downscaling daily observations using a stochastic method

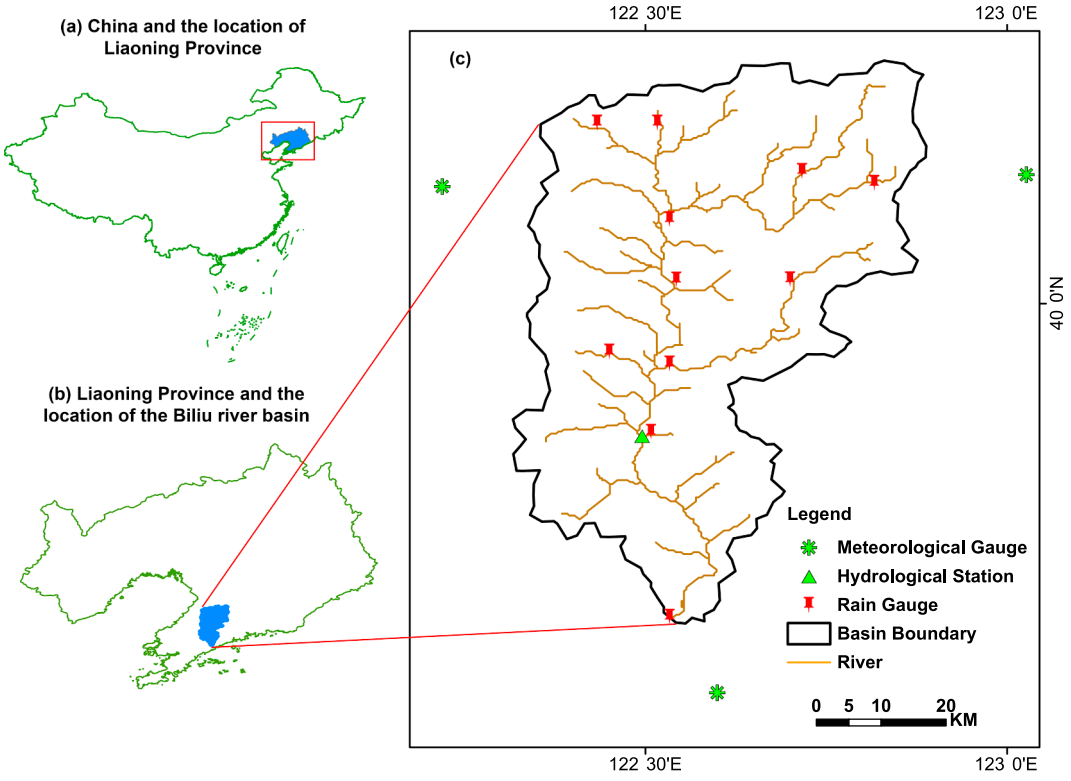

Fig. 3. The Biliu river basin.

(Wang et al., 2011). Hourly air temperatures are calculated using daily maximum and minimum temperatures based on the TEMP model (Parton and Logan, 1981). The estimated temperatures are further evaluated using daily average temperatures. In addition, a lapse rate of 6.5 K/km is used to consider elevation differences between model cells and meteorological gauges. Downward solar radiation data are estimated from sunshine duration, temperatures and humidity using a hybrid model (Yang et al., 2006). Downward long wave radiation is from the Global Land Data Assimilation Systems (GLDAS) because there is no observation. Air pressure data are estimated according to

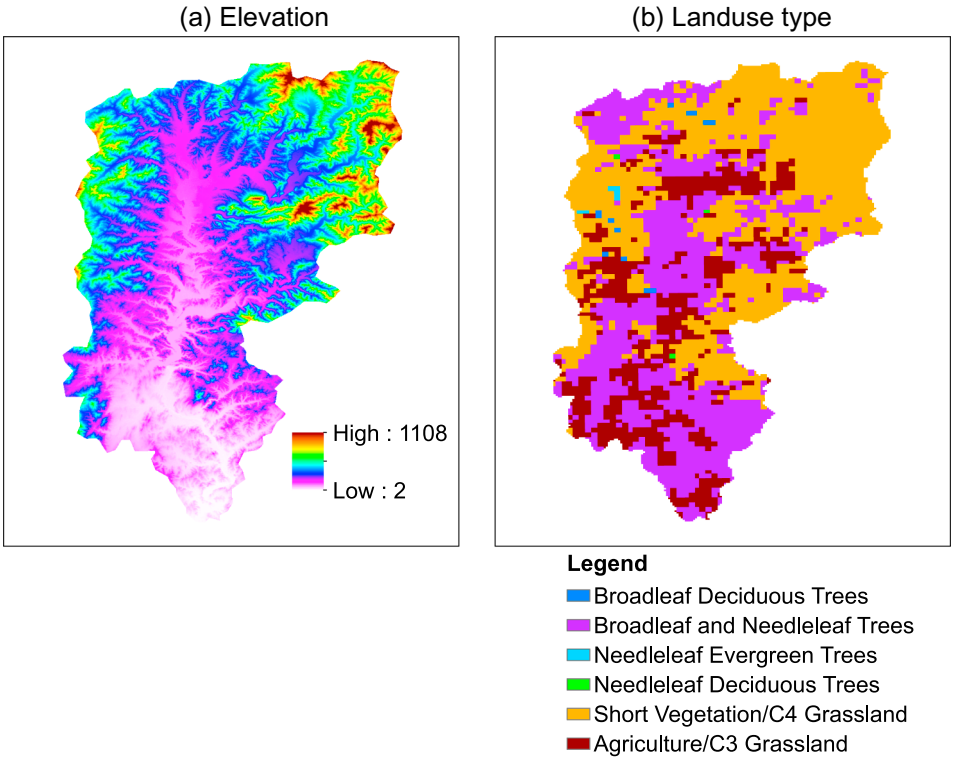

Fig. 4. Elevation (meters) and landuse types in the Biliu river basin.

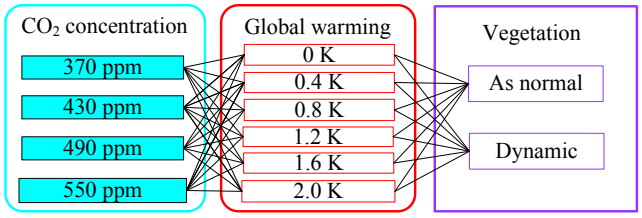

Fig. 5. Combinations of CO_2 concentration, global warming and vegetation condition scenarios.

elevation (Yang et al., 2006). This study region is the same as in the study by Qi et al. (2015), and more detailed descriptions about the data used, their processing and model parameter calibrations (including calibration approaches and calibrated values) can be found in the study by Qi et al. (2015).

3.3. Scenario datasets

Fig. 5 shows scenario settings for influence quantifications: combinations of the CO_2 concentration scenarios, temperature rise scenarios and vegetation scenarios. Four CO_2 concentration scenarios and six temperature rise scenarios are included considering the computational burden of V-WEB-DHM (two hours to finish one year simulation in a personal computer with four Inter Core i7-6700 3.40 GHz processors). The 'As normal' vegetation scenario means the MODIS LAI and FPAR data are used, and therefore the influences of leaf area changes when temperature and CO_2 concentration increase are not considered. The 'Dynamic' vegetation scenario means simulated LAI and FPAR under the assumed temperature and CO_2 concentration scenarios are utilized, and therefore the impacts of leaf area changes are considered.

Stern (2006) suggested that there are chances that global average temperature rise reaches 2 K when CO_2 concentration is 550 ppm, and that the temperature rise depends on general circulation models. Hansen et al. (2012) found that global temperature changes unevenly: there are some regions warming slower than the global average temperature rise. Many studies show future temperature rise under certain CO_2 concentration is uncertain because of large uncertainty of general circulation models (Fischer et al., 2013; Kharin et al., 2013; Chiyuan et al., 2014; Shiogama et al., 2016). In addition, many studies have suggested that solar radiation management approaches could effectively reflect sunlight back to space; therefore, temperature variations could be subjectively controlled under certain CO_2 concentration (Pongratz et al., 2012; Curry et al., 2014; Crook et al., 2015).

Thus, in this study, quantifying influences of increasing CO_2 concentration, temperature variations and leaf area changes are based on an assumption that different temperature rise values could happen under certain CO_2 concentration. These scenario settings are similar to the hypothetical sensitivity scenario methods used in previous studies (e.g., Rehana and Mujumdar, 2011; Wu et al., 2012a,b; Walling et al., 2017). Although the assumptions may be subjective, it enables to explore various potential consequences of increasing CO_2 concentration, temperature variations and leaf area changes, and therefore can provide an enhanced understanding of their impacts on water resources. In addition, it is assumed that temperatures in every month rise the same values. Therefore, differences in temperature rises in every month are not considered. Similar assumptions have been implemented in previous research (Ramirez and Finnerty, 1996; Streck, 2005; Arias et al., 2014).

On the basis of the above scenario settings, the parameters of ANOVA can be obtained, for example, H, K and L in Eqs. (6)–(10) equals six, four and two respectively; $\mathbf{g}$ in Eq. (4) is a $2 \times C_2^6 = 2 \times 15$ matrix; I in Eqs. (11)–(14) equals 15.

3.4. Assessment criteria for simulation

Four evaluation criteria were used for uncertainty assessment: Spearman's rank coefficient of determination (Rh^2), Pearson's linear coefficient of determination (R^2), Nash-Sutcliffe Efficiency (NSE) and relative bias (RB)

$$\begin{cases} Rh^2 = \left[1 - \frac{6 \cdot \sum d_i^2}{n \cdot (n^2 - 1)}\right]^2 \\ d_i = rank(X_{oi}) - rank(X_{si}) \end{cases} \quad (15)$$

$$R^2 = \frac{[\sum_{i=1}^{n} (X_{oi} - \bar{X}_o) \cdot (X_{si} - \bar{X}_s)]^2}{\sum_{i=1}^{n} (X_{oi} - \bar{X}_o)^2 \cdot \sum_{i=1}^{n} (X_{si} - \bar{X}_s)^2} \quad (16)$$

$$\mathrm{NSE} = 1 - \frac{\sum_{i=1}^{n} (X_{si} - X_{oi})^2}{\sum_{i=1}^{n} (X_{oi} - \bar{X}_o)^2} \quad (17)$$

$$\mathrm{RB} = \frac{\sum_{i=1}^{n} X_{si} - \sum_{i=1}^{n} X_{oi}}{\sum_{i=1}^{n} X_{oi}} \times 100\% \quad (18)$$

where X_{oi} represents observation or simulation using observed data; $\bar{X}_o$ represents average of observation or simulation using observed data; X_{si} represents simulation; $\bar{X}_s$ represents average of simulation; i represents time; n represents the total number of data points. A perfect fit should have Rh^2, R^2 and NSE values of one. The lower the |RB| values, the higher the accuracy. These criteria have commonly been used (e.g., Ebert et al., 2007; Wang et al., 2011; Qi et al., 2016d, 2018b), and therefore, they were used in this study.

4. Results

4.1. Vegetation dynamic simulation

Fig. 6 shows scatter plots of basin average MODIS LAI and climatic variables (including downward shortwave radiation, downward long wave radiation, relative humidity, air temperature and rainfall). Because the three SiB2 vegetation types (i.e., broadleaf and needleleaf trees, short vegetation/C4 grassland and agriculture/C3 grassland) account for over 98% of the Biliu river basin, plots for these three vegetation types are shown. Because local observed CO_2 concentration is not available, global monthly average values were used.

It can be seen that downward long wave radiation, relative humidity and air temperature show strong relationships with LAI variations, whereas shortwave radiation, rainfall and CO_2 spread out in the scatter plots. Because the relationships between LAI and climatic variables are non-linear, the correlations are analyzed using the Spearman's rank coefficient of determination which assesses how well the relationships can be described using monotonic functions. Rh^2 values are shown in Supplementary information Table S1. The results show the Rh^2 values of downward long wave radiation, relative humidity and air temperature are higher than others. Thus, downward long wave radiation, relative humidity and air temperature are considered in Eq. (3).

In this study, the DDS algorithm is used to calibrate the coefficients in Eq. (3) because DDS shows very good performance compared with others (Tolson et al., 2008a,b, 2009). R^2 is used as the objective function in calibrations with an evaluation number of the objective function values up to 10,000. The calibrations were repeated 10 times and 10 random seeds were used. The higher the R^2 values, the better the calibration. The coefficient values with the best R^2 value are selected. Because three environmental resources are selected to simulate LAI, n in Eq. (3) equals three, and therefore five parameters in Eq. (3) need to be calibrated. The lower and upper bounds of the five parameters are included in Supplementary information Section S1 and Supplementary information Table S2. The MODIS LAI data from 2000 to 2005 are used in the calibrations and data from 2006 to 2010 are used in validations. The equations to simulate LAI after calibrations are shown in Eqs.

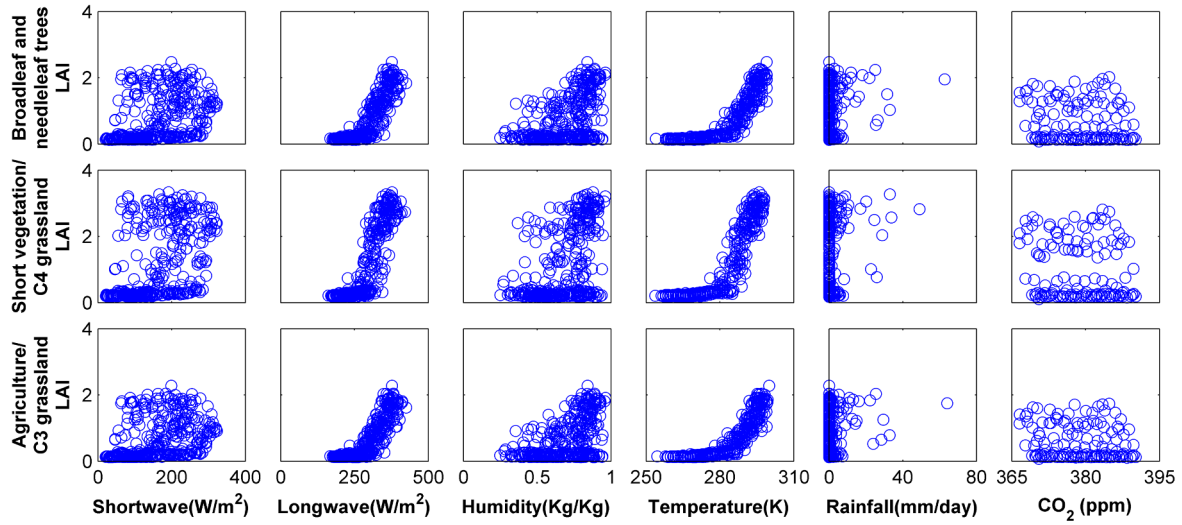

Fig. 6. Scatter plots of basin average MODIS LAI and climatic variables. 496 data pairs (from March 2000 to December 2010) are utilized for downward shortwave radiation, down ward long wave radiation, relative humidity, temperature and rainfall. 130 data pairs (from March 2000 to December 2010) are used for CO_2 since monthly scale data is used, and correspondingly the monthly average LAI values are utilized to draw the scatter plots.

(19)–(21):

$$LAI_{broad-needle\ leaf\ trees} = \frac{7.5454}{1 + \exp[30.4909 - (1.5995\cdot10^{-5}\cdot R_{lw} + 7.1938\cdot10^{-3}\cdot Rh + 9.7239\cdot10^{-2}\cdot T_{air})]} \quad (19)$$

$$LAI_{short\ vegetation/C4\ grassland} = \frac{8.1445}{1 + \exp[29.99 - (2.9988\cdot10^{-5}\cdot R_{lw} + 6.4994\cdot10^{-3}\cdot Rh + 9.7443\cdot10^{-2}\cdot T_{air})]} \quad (20)$$

$$LAI_{agriculture/C3\ grassland} = \frac{7.1615}{1 + \exp[30.4929 - (1.3997\cdot10^{-5}\cdot R_{lw} + 8.6683\cdot10^{-3}\cdot Rh + 9.6078\cdot10^{-2}\cdot T_{air})]} \quad (21)$$

where R_{lw} represents downward long wave radiation; Rh represents relative humidity; T_{air} represents air temperature.

On the basis of Eqs. (19)–(21), it can be seen that T_{air} is the main constrains of LAI increase: T_{air} has higher coefficient values than Rh and R_{lw}. The results are consistent with previous studies. For example, Nemani et al. (2003) and Yao et al. (2018) also identified temperature as the main limit of vegetation growth in the study region of this paper. Therefore, the approach used in calculating coefficient values is acceptable, and the calibrated parameter values are appropriate.

4.2. Validations of vegetation dynamic simulation

Fig. 7 shows the NSE and RB values. They represent the differences between simulated LAI and MODIS 8-day LAI. The NSE values are above 0.67, 0.84 and 0.92 on daily, monthly and mean monthly scales, respectively. The absolute values of RB are less than 14%. Therefore, the simulated LAI values replicate MODIS LAI well. Comparison between simulated LAI and MODIS LAI in time series plots are shown in Supplementary information Figs. S1 and S2.

In addition to LAI, FPAR data is also needed in V-WEB-DHM. The FPAR calculation procedures can be found in Supplementary information Section S2. Fig. 8 shows spatial distribution comparison of mean monthly LAI and FPAR for major growing seasons (from April to October); Fig. S8 shows multi-year mean monthly differences. LAI and FPAR have the largest values in July and August for the MODIS data.

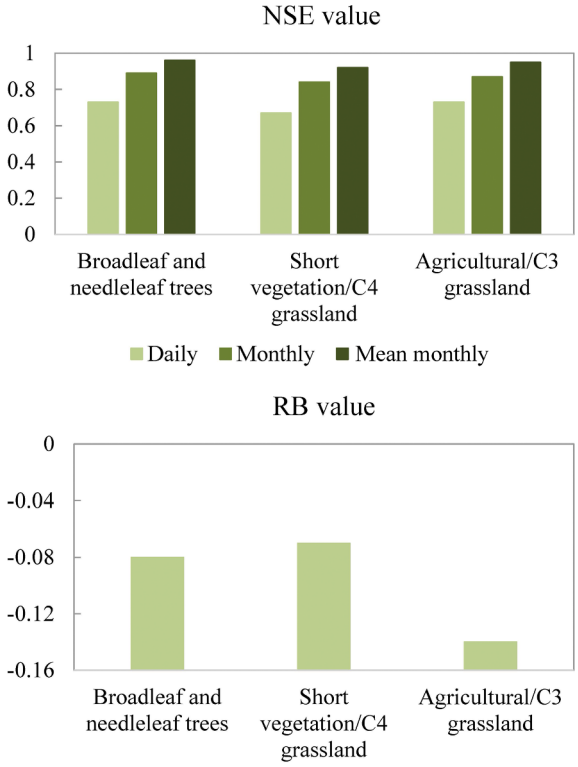

Fig. 7. NSE and RB values of simulated LAI. The NSE and RB values are calculated on the basis of simulated LAI and MODIS products.

Similarly, simulated LAI and FPAR also show higher values in July and August. Regarding spatial distributions, simulated LAI and FPAR values can replicate observed distributions of MODIS data: larger values in northern mountainous regions and smaller in southern plains. In a few high/low elevations (Fig. S8), the differences between MODIS and simulated data become higher. These uncertainties may result from input data uncertainty of V-WEB-DHM, such as homogeneous lapse rate of temperatures (6.5 K/km) and downward long wave radiation of GLDAS. In addition, the calibrated coefficients of LAI and FPAR simulation equations may contribute to the uncertainty. Overall, the simulations agree well with MODIS observations.

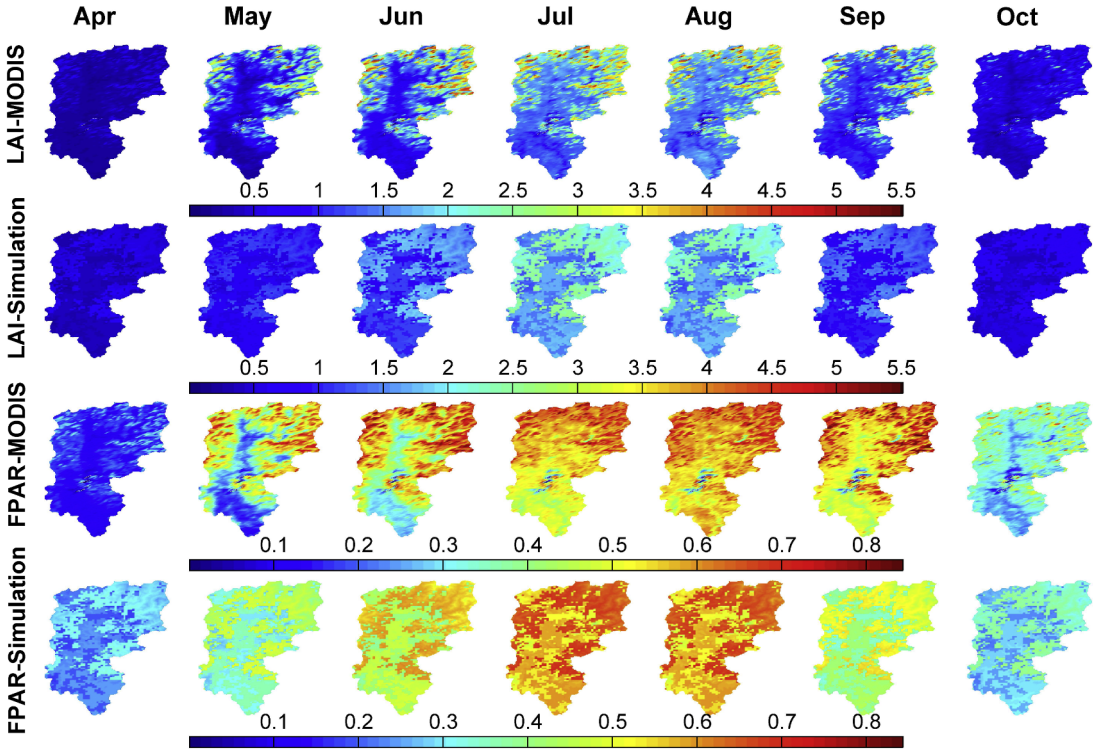

Fig. 8. Comparison of mean monthly LAI and FPAR between simulated values and MODIS observation in the main growing periods (from April to October).

4.3. Validations of water and energy flux simulations

Fig. 9a, c and e show simulated runoff results using MODIS LAI and FPAR, observed relative humidity and GLDAS downward long wave radiation. On a daily scale, simulated runoff using observed data agrees well with observed runoff: the overall NSE and RB are 0.68 and −9%. The NSE and RB values are up to 0.88 and −9% on a monthly scale (Fig. 9c). Similarly, simulation shows very good performance on a multi-year mean monthly scale, with NSE values being 0.89 (Fig. 9e). Fig. 9b, d and f show simulated runoff using simulated LAI, FPAR, relative humidity and downward long wave radiation. On a daily scale, the simulated runoff replicates observed values well, with NSE and RB being 0.69 and −11%, respectively (Fig. 9b). On monthly and multi-year mean monthly scales, the NSE values are up to 0.85 (Fig. 9d and f). The NSE values of V-WEB-DHM simulations on daily and monthly scales are a little better than WEB-DHM simulations, which may be because WEB-DHM uses 8-day MODIS data and V-WEB-DHM uses simulated daily scale LAI and FPAR data. Overall, these results indicate that V-WEB-DHM can effectively simulate hydrological processes in the Biliu river basin.

Fig. 10 shows temporal variations and spatial distributions of fluxes simulated by WEB-DHM and V-WEB-DHM, and Fig. S9 in the Supplementary information shows multi-year mean differences (results of V-WEB-DHM minus results of WEB-DHM). Average values for four time periods are shown. Four flux data are compared, including land surface temperatures (Fig. 10a and c), ET (Fig. 10b and d), surface soil wetness (Fig. 10e and g) and root zone wetness (Fig. 10f and h). Temporal variations and spatial distributions of LSTs agree well. Similarly, temporal variations and spatial distributions of ET, surface zone wetness and root zone wetness also agree well overall but with exceptions in several high/low elevations (Fig. S9). Here, these exceptions may also be due to uncertainties in input data and calibrated coefficients of LAI and FPAR simulation equations. Overall, the simulations of WEB-DHM and V-WEB-DHM agree relatively well.

4.4. Impact quantification

After evaluations with observed runoff, water fluxes, energy fluxes, MODIS LSTs, LAI and FPAR, V-WEB-DHM demonstrates its good performance in representing water, energy and vegetation dynamic processes in the Biliu river basin. Thus, V-WEB-DHM is used in this section to investigate the respective and combination impacts of increasing CO_2 concentration, temperature variations and leaf area changes on water resources. It should be noted that the quantified impacts here do not necessarily represent the model errors, but represent the variations of hydrological variables and land surface fluxes from present model simulations based on observed data.

Fig. 11 shows mean monthly contributions of CO_2 concentration changes, temperature variations and leaf area changes to the variations of basin average variables. The bandwidth represents overall variations generated from the $4 \times 6 \times 2$ scenarios shown in Fig. 5. It can be seen that changes in CO_2 concentration, temperature and leaf area have considerable influences on simulated variables: generating large bandwidth.

For canopy transpiration, in July, leaf area changes have larger impacts than in other months (account for 41.31%), and the physiological effects of CO_2 concentration changes (account for 37.14%) are lower than influence of leaf area changes; in May, June and August, the physiological effects of CO_2 concentration changes have larger impacts than others. The temperature in July is higher than other months, which may result in leaf area changes have higher impact on canopy transpiration than the physiological effects of CO_2 concentration changes. The influence of temperature changes on canopy transpiration is larger in May, June, July and August than other months. This may be because temperature provides essential conditions to keep the enzyme working when chlorophyll is increasing in these months. In September and October, the chlorophyll in leaves is reducing, and therefore the influence of temperature changes decreases. In the beginning of the growing season (April), LAI is smaller compared with other months (as shown in Fig. 8), and therefore the effects of the CO_2 concentration and

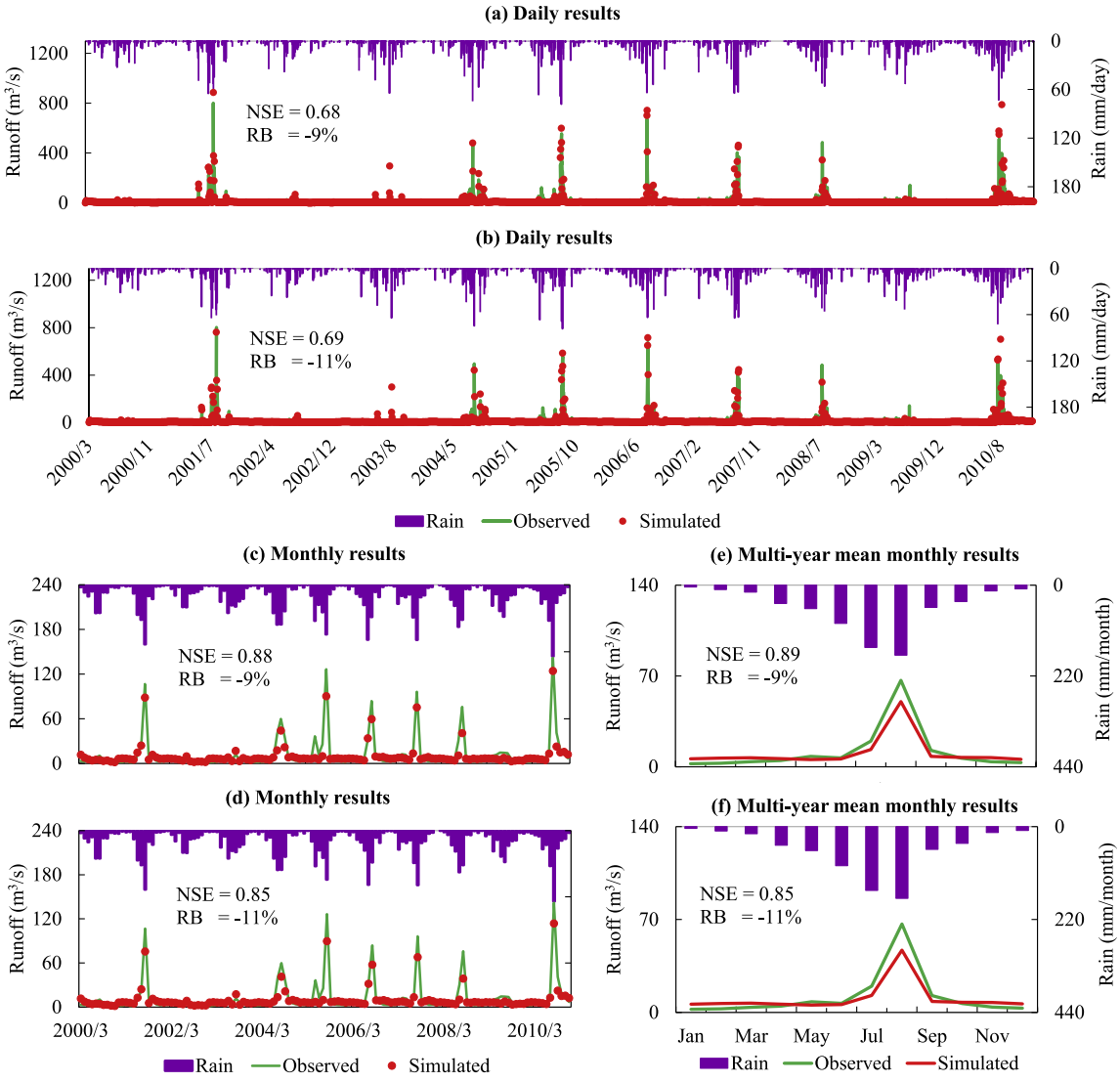

Fig. 9. Observed and simulated runoff in the Biliu river basin from March 2000 to December 2010. (a), (c) and (e): results using MODIS LAI and FPAR, observed relative humidity and GLDAS downward long wave radiation; (b), (d) and (f): results using simulated LAI, FPAR, relative humidity and downward long wave radiation.

temperature changes are smaller than other months, whereas it may be due to decrease in chlorophyll in September and October. The higher influence of leaf area changes than CO_2 concentration and temperature changes in April and September may result from higher LAI compared with the 'As normal' scenario. Moreover, it can be seen that the combinations of increasing CO_2 concentration, global warming and leaf area changes have little influence on runoff, soil wetness, stomatal conductance and net primary productivity.

Regarding the average influence from April to October on canopy transpiration, the sum of the average influences of leaf area changes and temperature variations is 59.27%, which is more than 1.6 times higher than the average influence of CO_2 (36.97%). Similar to the canopy transpiration, the sum of the average influences of leaf area and temperature variations is higher than CO_2 for surface zone wetness, root zone wetness and net primary productivity of C4 plants. For other variables, the leaf area changes and increasing CO_2 concentration have considerable influence, implying that it is necessary to consider changes in CO_2 concentration and leaf area in hydrological simulation under climate change.

Fig. 12(a) and (b) shows simulated runoff of the 'Dynamic' vegetation scenario; Fig. 12(c) shows mean monthly contributions of increasing CO_2 concentration, temperature variations and leaf area changes to runoff variations..

Fig. 12(a) shows runoff is decreasing overall, which may result from increasing ET. Fig. 12(b) shows the influence on runoff in August. The runoff is increasing with increasing CO_2 concentration, and decreasing with increasing temperature. This is because the increased ET caused by temperature rises is higher than decreased ET caused by increasing CO_2 concentration, and therefore ET is increasing overall. Fig. 12(c) shows leaf area changes are the dominator of runoff changes in August, which may be because the total influence of leaf area variations on ET, surface zone wetness and root zone wetness are higher than influences of CO_2 concentration and temperature changes (as shown in Table 1). In Fig. 11, leaf area changes have the largest impacts on canopy transpiration and ET in July. This difference between Figs. 11 and 12(c) may be because leaf area changes have higher impact on surface zone wetness in August than in July (as shown in Fig. 11). Surface zone wetness represents water storage in soil and therefore its changes can lead to runoff variations. Fig. 12 shows the combinations have little influence on the runoff variations, which is similar to Fig. 11.

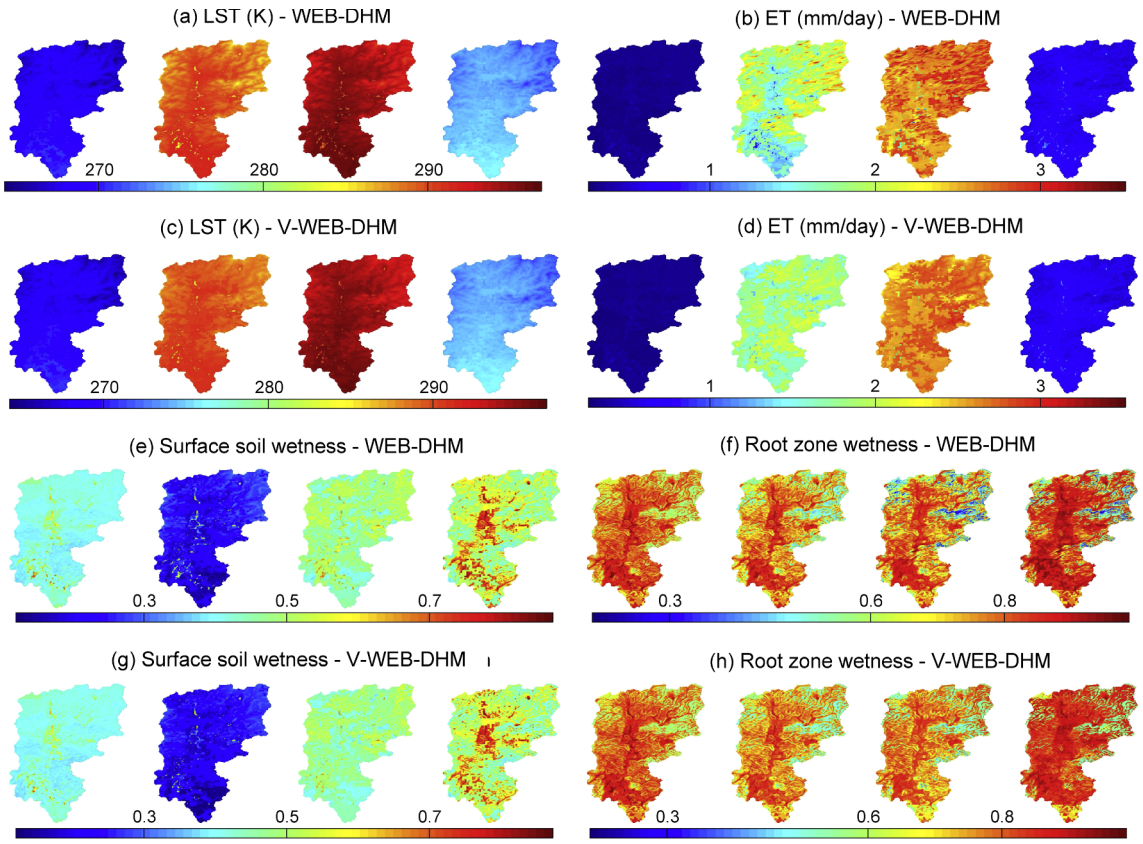

Fig. 10. Temporal variation and spatial distribution comparisons of simulated mean water and energy fluxes between V-WEB-DHM and WEB-DHM. JFM, AMJ, JAS, and OND are listed from left to right.

5. Discussion

5.1. Comparison with other studies

Sawada et al. (2014) integrated a vegetation module into WEB-DHM, and used it in drought analysis. However, the impacts of elevated CO_2 concentration, rising temperature and vegetation dynamics on water resources were not quantified in the study by Sawada et al. (2014). In our study, the individual and combination impacts of them are explicitly quantified using a framework integrating V-WEB-DHM and ANOVA. It is necessary to quantify their relative influences because it can provide very useful information on main influential factors, and therefore measures can be taken to avoid negative influence by controlling the main factors. At the same time, the quantification can also provide insight into the importance of considering some influential factors in hydrological simulation and drought analysis under climate change, such as vegetation dynamics which are frequently neglected in basin scale hydrological model simulations.

Previous studies have investigated the influences of temperature, CO_2 concentration and/or vegetation changes on runoff (Labat et al., 2004; Gedney et al., 2006; Leipprand and Gerten, 2006; Piao et al., 2007; Gerten et al., 2008; Cheng et al., 2014; Tao et al., 2014; Tesemma et al., 2015). However, few studies have been carried out to quantify the relative influences of them and their combination influences on a river basin scale. This could be because there is a lack of a comprehensive framework that can simulate and quantify vegetation dynamics, photosynthesis-conductance changes, biosphere hydrological processes and relative influences of them on a river basin scale. However, in this paper, a distributed biosphere hydrological model with a dynamic vegetation module is developed and a comprehensive framework combining the developed model and a sensitivity analysis approach is proposed. This framework facilitates the simulation and quantification of the individual and combination effects on a river basin scale. Using the framework we found the sum of the influences of leaf area and temperature changes on canopy transpiration is more than 1.6 times higher than influence of CO_2 concentration changes in main growing seasons. This result implies transpired water with global warming and LAI variations could be more than conserved water due to suppressed transpiration by elevated CO_2 concentration. Few studies have reported similar results in this region.

Gedney et al. (2006) found the individual effects of climate, aerosol concentration, CO_2 concentration and land use type changes on runoff can be combined linearly to represent their total influence, which implies their combination influence is little. Lemordant et al. (2018) found radiative and physiological effects of CO_2 concentration changes on evaporative fraction can be combined linearly. Different from the studies by Gedney et al. (2006) (in which LAI changes were not explicitly considered) and Lemordant et al. (2018), our study found the combination influence of temperature, CO_2 concentration and leaf area changes is little compared with their individual effects, which has rarely been explicitly and quantitatively reported according to the best of the authors' knowledge. This finding could provide useful information to the current limited pool of knowledge regarding the influence of increasing CO_2 concentration, temperature variations and vegetation changes on water resources on a river basin scale.

We found increasing CO_2 concentration can increase runoff, and increasing temperature decreases runoff in the studied region. This founding is different from the research by Piao et al. (2007), in which it is found increasing CO_2 concentration can reduce runoff when considering CO_2 fertilization effects. The difference may be because the study by Piao et al. (2007) utilized globally average runoff and CO_2 fertilization effects are not significant in our study, implying that CO_2 effects are different in different regions. Lemordant et al. (2016) suggested that elevated CO_2 concentration could increase soil moisture,

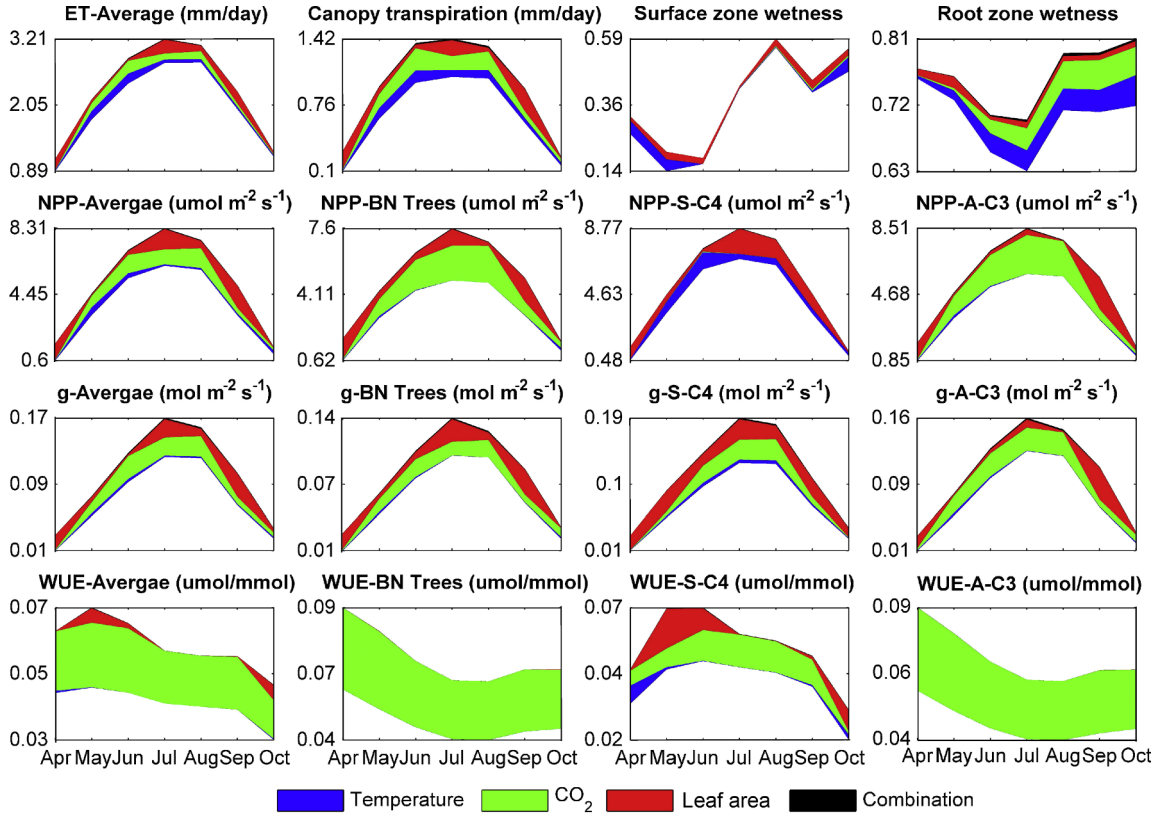

Fig. 11. Mean monthly contributions (from April to October) of CO_2 concentration, temperature and leaf area changes to variations of basin average ET, canopy transpiration, surface zone wetness, root zone wetness, NPP, stomatal conductance (g) and water use efficiency (WUE). 'BN Trees' represents broadleaf and needleleaf trees; 'S-C4' represents short vegetation/C4 grassland; 'A-C3' represents agriculture/C3 grassland.

and Betts et al. (2007) suggested that increased soil moisture could increase runoff. Dai (2013) suggested increasing temperature can increase drought severity. Swann et al. (2016) suggested that increasing temperature reduces water resources availability, and the severity of drought is reduced when considering the influence of elevated CO_2 concentration. These studies appear to support our results. Nevertheless, our study was carried out in an important medium-sized river basin, which is challenging for the approaches used in the previous studies because of the coarse resolutions of Earth System Models (ESM) and global circulation models they used.

Jasechko et al. (2013) showed transpiration from vegetation is the largest water flux on Earth's continents and accounts for 80%-90% of terrestrial evapotranspiration. Lemordant et al. (2018) found water resources availability will be strongly modified by vegetation physiological effects in response to elevated CO_2 concentration, and influence of precipitation changes on drought is lower than previous expectation. Lian et al. (2018) found that the vegetation responses to climate change is more important to water resources availability projections than previously thought. Most basin scale hydrological models currently do not consider transpiration in vegetation leaf. Therefore, water resources availability projections could be problematic when using them. In our study, we considered the influence of vegetation changes on runoff by developing the vegetation simulation module, and found leaf area changes have the largest influence on runoff (as shown in Fig. 12c). Our results are consistent with the previous studies. Nevertheless, we also show the differences of the leaf area changes influences in different months, which are not investigated in the previous studies.

5.2. Comments on the developed framework

LAI variations depend on availability of environmental resources, and influence of resources is different in various regions (Jolly et al., 2005; Orlandi et al., 2013; Hwang et al., 2014; Reich et al., 2014; Wang-Erlandsson et al., 2014). For example, Donohue et al. (2013) suggested that water could be a main resource influencing vegetation growth in warm and arid regions; Yang et al. (2016) suggested that radiation and nutrients are main resources influencing vegetation growth in warm and humid regions. Yao et al. (2018) studied climate influence on gross primary productivity variations in China, and also identified temperature as a main influential factor in the study region in our paper, which seems to support our study. As shown in Eqs. (1) and (2), Rh can influence canopy conductance and transpiration, which are related to vegetation growth, and therefore Rh is considered in LAI simulations in Eqs. (19)–(21). Hesketh and Warrington (1989) also suggested that humidity could influence seedling emergence and leaf area expansion, and therefore can influence LAI. Moreover, the study region has a temperate monsoon marine climate, and growing seasons are mainly controlled by temperature (Nemani et al., 2003). Thus, the three climatic variables chosen in this study are acceptable for LAI simulation.

There are several approaches that simulate LAI based on daily scale hydro-climatic data. For example, growing degree-days approaches simulate LAI based on daily temperatures (Miller et al., 2001; Koetz et al., 2005; Setiyono et al., 2008; Cao et al., 2015); Growing Season Index (GSL) approaches utilize daily scale photoperiod, vapor pressure and minimum temperatures to model LAI (Jolly et al., 2005; Savoy and Mackay, 2015); a variant of the GSL approach implements day length, daily scale minimum temperatures and soil moisture (Wang-Erlandsson et al., 2014). In these prior studies, the hydro-climatic variables used have similar monthly fluctuations with LAI. Therefore, it is acceptable to simulate LAI based on climatic variables that have similar monthly variations as LAI.

LAI dynamics can be modelled using a few methods, for example, approaches on the basis of exponential distributions considering

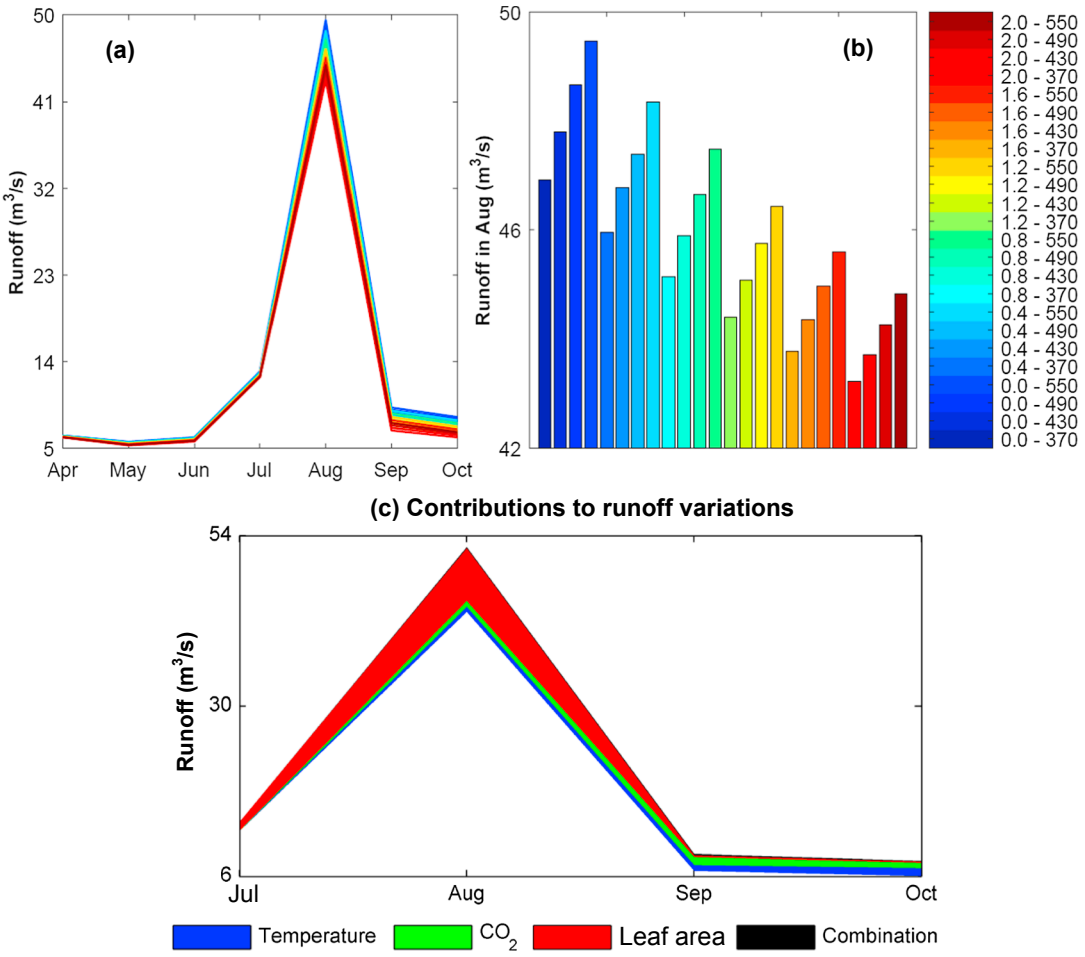

Fig. 12. (a) Simulated runoff; (b) simulated runoff in August in bar plot; (c) mean monthly contributions of CO_2 concentration, temperature and leaf area changes to runoff variations. The different colors in (a) and (b) represent the temperature rise and CO_2 concentration values (as shown in Fig. 5) which are used as V-WEB-DHM inputs when simulating runoff variations.

Table 1
Influences of leaf area, CO_2 concentration and temperature changes on ET, root zone wetness and surface zone wetness in August.

Influence factor	Influence			Total influence
	ET	Root zone wetness	Surface zone wetness	
Leaf area changes	0.32	0.09	0.8	1.21
eCO_2	0.44	0.48	0.11	1.03
Temperature changes	0.19	0.38	0.08	0.65

Note. 'Total influence' represents the sum of the influences on ET, root zone wetness and surface zone wetness; eCO_2 = elevated CO_2 concentration. The influence is quantified based on Eqs. (4)–(14).

temperature, relative humidity, etc. (Cao et al., 2015; Tesemma et al., 2015); approaches allocating carbon resources to leaves, stems and roots (Cox, 2001; Sitch et al., 2003; Clark et al., 2011). The overall objective of this research is to simulate changes in river runoff. Although an exponential function is used in this study to estimate LAI without explicitly considering carbon allocations, the runoff simulation results are acceptable (recall the results in Fig. 9). In addition, validations using MODIS LAI shows the simulated LAI replicates observation well (recall the results in the Section 4.2). Therefore, the LAI simulation approach in this study is acceptable.

Regarding CO_2 influence on LAI, Eq. (3) is a general form and can consider CO_2 impacts on LAI. However, fertilization effects of CO_2 are changing in different regions and studies have shown the fertilization effects may not exist in some regions (e.g., Yang et al., 2016; Zhu et al., 2016; Duursma et al., 2016). In our case study region, there are two reasons that we do not consider the fertilization effects: (i) fertilization effects of CO_2 are not considerable in our study region as shown in a quantitative research by Zhu et al. (2016); (ii) the study by Nemani et al. (2003) and Yao et al. (2018) revealed temperature is a main driver of vegetation variations in our study region. When studies are carried out in regions with CO_2 fertilization, there are two approaches to incorporate CO_2 fertilization into Eq. (3): (i) considering CO_2 as an influential factor in the denominator of Eq. (3); (ii) considering CO_2 influence on LAI_{max} in the numerator of Eq. (3) as pointed out by Donohue et al. (2013) that CO_2 fertilization effects could influence maximum vegetation coverage. Because CO_2 fertilization effects on LAI are still at the forefront of research, more studies are encouraged in the future to incorporate this influence into Eq. (3).

The overall objective of this study is to investigate changes in water resources. The LAI simulation approach was calibrated using MODIS LAI from 2000 to 2005, and validated from 2006 to 2010 based on MODIS LAI. Both the calibration and validation results show acceptable performance with NSE and absolute values of RB being over 0.73 and less than 14% (recall the results in Fig. 7). In addition, the validations using observed runoff show the model can simulate runoff well using simulated LAI. Therefore, it is assumed that the model is appropriate to predict changes in runoff. Similar assumption has also been utilized in previous studies (e.g., Miller et al., 2001; Koetz et al., 2005; Setiyono et al., 2008; Cao et al., 2015; Su et al., 2015; Tesemma et al., 2015).

In this study, R^2 is utilized to represent differences between simulated LAI and MODIS LAI. The higher the R^2 values, the better the calibrated parameters. Therefore, the calibration is to maximize R^2. Although only R^2 is used, the calibrated parameters show good performance in replicating MODIS LAI. The limited length of meteorological data used (2000–2010) may influence the analysis in this study. However, the V-WEB-DHM model is applicable even when study data changes. Although empirical functions are established to estimate FPAR from LAI in this study, other approaches simulating FPAR based on LAI are applicable as well, for example, the Beer's law (Monsi and Saeki, 1953; Bondeau et al., 2007). In our study region, human abstracts water mainly from the Biliu reservoir, which could not influence the reservoir inflow. Therefore, influence of human water abstractions was not considered.

5.3. Limitations

In this study, possible changes in vegetation height and diameter were not considered. Water vapour in the atmosphere may change when vegetation varies, which may increase cloud and then may raise solar radiation reflection by cloud. These changes were not considered. Other greenhouse gases, such as methane and nitrous oxide, were not considered. With changes in temperature and CO_2 concentration, plant rooting depth may increase, which allows plant to access soil moisture at deeper layers, especially during dry spells. In this study, we used prescribed rooting depth in SiB2 and therefore the changes in rooting depth when CO_2 and temperature changes were not considered. As interactions between eCO_2, climate, water cycle and rooting depth are still at the forefront of research (as shown in a recent debate between Fan et al. (2017) and Pierret and Lacombe (2018)), more studies are encouraged in the future to consider the influence of rooting depth. Other influential factors were not considered, such as vapour pressure (Willett et al., 2008; Fatichi et al., 2015), wind speed (McVicar et al., 2012; Schymanski and Or, 2016) and net radiation changes (i.e., dimming and brightening) (Wild et al., 2005; Mercado et al., 2009; Wild, 2009). Vegetation influences on CO_2 concentration, global warming and precipitation were not considered. To consider these effects, more complex ESMs should be used, which is very difficult at present in a medium-sized river basin because of coarse resolutions of ESMs. Without considering these effects, the total variance may be underestimated. Future research is encouraged when fine resolution ESM data is available.

In this study, it is assumed that precipitation is enough to sustain vegetation growth in different CO_2 concentration and temperature rise scenarios because the objective of this research is to quantify the influences of CO_2 concentration, temperature and vegetation changes on water resources. Precipitation may change under the different scenarios, and the changes were not considered in this study. Future studies are encouraged to consider precipitation changes using fine resolution precipitation simulation of ESMs. Air temperature lapse rates may vary within a year and also relate to vapour pressure and wind speed (McVicar et al., 2007). A lapse rate of 6.5 K/km was used in this study, which may contribute to the uncertainty in simulated results. Future research is encouraged to utilize more sophisticated data when detailed lapse rates are available.

6. Conclusions

Increasing CO_2 concentration, global warming and vegetation changes have profound influence on regional water resources. However, quantitative assessments of their respective and combination influences on river basin scales remain few, especially in northeast China. A better understanding of the complex influence can help develop measures to ameliorate regional water resources challenges. This study presents an important progress in quantifying the influences of the three key driving forces of water resource changes. The major contributions are summarized as follows based on this study.

First, a dynamic vegetation simulation approach is developed and incorporated into WEB-DHM. Therefore, the influences of increasing CO_2 concentration, temperature variations, vegetation changes and their combinations on water resources can be simulated.

Second, a comprehensive framework is proposed by integrating V-WEB-DHM and a variance-based sensitivity analysis approach. This new framework enables quantification of the influences of changes in CO_2 concentration, temperature, vegetation and their combinations using values between zero and one: revealing the relative importance of them.

Third, we find sum of the influences of LAI and temperature variations on canopy transpiration is larger than physiological effects of CO_2. This finding implies transpired water could be more than conserved water with elevated CO_2 concentration, global warming and leaf area changes. Therefore, considering changes in temperature and LAI are of importance in projections of future water resources.

Fourth, we also find LAI dynamics play a dominate role in runoff decreases in hot summer. This result implies that water resources availability could be overestimated in summer if LAI changes are neglected. Therefore, severity of future water shortage could be underestimated if LAI changes are not taken into considerations.

In the future, the proposed approaches could be applied in other sizes/types of studies (e.g., all China) to investigate influences of elevated CO_2 concentration, rising temperature and vegetation dynamics on water resources.

Declaration of interest

None.

Acknowledgements

This study was supported by the National Natural Science Foundation of China (41625001, 51809136), and China Postdoctoral Science Foundation (2017M622516). Monthly average CO_2 data were obtained from ftp://aftp.cmdl.noaa.gov/products/trends/co2/co2_mm_gl.txt. The data of the Biliu river basin were collected from the Biliu reservoir administration.

Appendix A. Supplementary data

Supplementary data to this article can be found online at https://doi.org/10.1016/j.jhydrol.2019.01.015.

References

Arias, R., Rodríguez-Blanco, L.M., Taboada-Castro, M.M., Nunes, J., Keizer, J., Taboada-Castro, T.M., 2014. Water resources response to changes in temperature, rainfall and CO_2 concentration: a first approach in NW Spain. Water 6 (10), 3049–3067.

Baker, H.S., et al., 2018. Higher CO_2 concentrations increase extreme event risk in a 1.5 °C world. Nat. Clim. Change 8 (7), 604–608.

Ball, J.T., 1988. In: An Analysis of Stomatal Conductance. Stanford University, pp. 89.

Betts, R.A., et al., 2007. Projected increase in continental runoff due to plant responses to increasing carbon dioxide. Nature 448 (7157), 1037–1041.

Bondeau, A., Smith, P.C., Zaehle, S., 2007. Modelling the role of agriculture for the 20th century global terrestrial carbon balance. Glob. Change Biol. 13 (3), 679–706.

Bosshard, T., Carambia, M., Goergen, K., Kotlarski, S., Krahe, P., Zappa, M., Schär, C., 2013. Quantifying uncertainty sources in an ensemble of hydrological climate-impact projections. Water Resour. Res. 49 (3), 1523–1536.

Cao, X., Zhou, Z., Chen, X., Shao, W., Wang, Z., 2015. Improving leaf area index simulation of IBIS model and its effect on water carbon and energy—a case study in Changbai Mountain broadleaved forest of China. Ecol. Model. 303, 97–104.

Cheng, L., Zhang, L., Wang, Y.-P., Yu, Q., Eamus, D., O'Grady, A., 2014. Impacts of elevated CO_2, climate change and their interactions on water budgets in four different catchments in Australia. J. Hydrol. 519, 1350–1361.

Chiyuan, M., Qingyun, D., Qiaohong, S., Yong, H., Dongxian, K., Tiantian, Y., Aizhong, Y., Zhenhua, D., Wei, G., 2014. Assessment of CMIP5 climate models and projected temperature changes over Northern Eurasia. Environ. Res. Lett. 9 (5), 055007.

Clark, D.B., et al., 2011. The Joint UK Land Environment Simulator (JULES), model description – part 2: carbon fluxes and vegetation dynamics. Geosci. Model Dev. 4 (3),

701–722.
Collatz, G.J., Ribas-Carbo, M., Berry, J.A., 1992. Coupled photosynthesis-stomatal conductance model for leaves of C4 plants. Funct. Plant Biol. 19 (5), 519–538.
Collatz, J.G., Ball, T.J., Grivet, C., Berry, J.A., 1991. Physiological and environmental regulation of stomatal conductance, photosynthesis and transpiration: a model that includes a laminar boundary layer. Agric. For. Meteorol. 107–136.
Cox, P.M., 2001. TRIFFID Dynamic Global Vegetation Model, Hadley Centre Technical Note 24. Hadley Centre, Bracknell, U.K.
Crook, J.A., Jackson, L.S., Osprey, S.M., 2015. A comparison of temperature and precipitation responses to different Earth radiation management geoengineering schemes. J. Geophys. Res.: Atmospheres 120 (18), 9352–9373.
Curry, C.L., et al., 2014. A multimodel examination of climate extremes in an idealized geoengineering experiment. J. Geophys. Res.: Atmospheres 119 (7), 3900–3923.
Dai, A., 2013. Increasing drought under global warming in observations and models. Nat. Clim. Change 3 (1), 52–58.
Deb, K., Gupta, H., 2006. Introducing robustness in multi-objective optimization. Evol. Comput. 14 (4), 463–494.
Donohue, R.J., Roderick, M.L., McVicar, T.R., Farquhar, G.D., 2013. Impact of CO_2 fertilization on maximum foliage cover across the globe's warm, arid environments. Geophys. Res. Lett. 3031–3035.
Donohue, R.J., Roderick, M.L., McVicar, T.R., Yang, Y., Donohue, R.J., Roderick, M.L., McVicar, T.R., Yang, Y., 2017. A simple hypothesis of how leaf and canopy-level transpiration and assimilation respond to elevated CO_2 reveals distinct response patterns between disturbed and undisturbed vegetation. J. Geophys. Res. Biogeosci. 122, 168–184.
Duan, Q., Gupta, V.K., Sorooshian, S., 1993. Shuffled complex evolution approach for effective and efficient global minimization. J. Optim. Theory Appl. 73 (3).
Duursma, R.A., Gimeno, T.E., Boer, M.M., Crous, K.Y., Tjoelker, M.G., Ellsworth, D.S., 2016. Canopy leaf area of a mature evergreen Eucalyptus woodland does not respond to elevated atmospheric [CO_2] but tracks water availability. Glob. Change Biol. 22 (4), 1666–1676.
Ebert, E.E., Janowiak, J.E., Kidd, C., 2007. Comparison of near-real-time precipitation estimates from satellite observations and numerical models. Bull. Am. Meteorol. Soc. 88 (1), 47–64.
Fan, Y., Miguez-Macho, G., Jobbágy, E.G., Jackson, R.B., Otero-Casal, C., 2017. Hydrologic regulation of plant rooting depth. Proc. Natl. Acad. Sci. 114 (40), 10572–10577.
Fatichi, S., Molnar, P., Mastrotheodoros, T., Burlando, P., 2015. Diurnal and seasonal changes in near-surface humidity in a complex orography. J. Geophys. Res.: Atmospheres 120 (6), 2358–2374.
Field, C.B., Jackson, R.B., Mooney, H.A., 1995. Stomatal responses to increased CO_2: implications from the plant to the global scale. Plant Cell Environ. 18 (10), 1214–1225.
Fischer, E.M., Beyerle, U., Knutti, R., 2013. Robust spatially aggregated projections of climate extremes. Nat. Clim. Change 3 (12), 1033–1038.
Gedney, N., Cox, P.M., Betts, R.A., Boucher, O., Huntingford, C., Stott, P.A., 2006. Detection of a direct carbon dioxide effect in continental river runoff records. Nature 439 (7078), 835–838.
Gerten, D., Rost, S., von Bloh, W., Lucht, W., 2008. Causes of change in 20th century global river discharge. Geophys. Res. Lett. 35 (20).
Greve, P., Gudmundsson, L., Seneviratne, S.I., 2018. Regional scaling of annual mean precipitation and water availability with global temperature change. Earth Syst. Dyn. 9 (1), 227–240.
Hansen, J., Sato, M., Ruedy, R., 2012. Perception of climate change. Proc. Natl. Aacd. Sci. 109 (37), 23.
Hansen, M.C., et al., 2013. High-resolution global maps of 21st-century forest cover change. Science 342 (6160), 850.
Hesketh, J.D., Warrington, I.J., 1989. Corn growth response to temperature: rate and duration of lead emergence. Agron. J. 81 (4), 696–701.
Hu, Z., Wang, L., Wang, Z., Hong, Y., Zheng, H., 2015. Quantitative assessment of climate and human impacts on surface water resources in a typical semi-arid watershed in the middle reaches of the Yellow River from 1985 to 2006. Int. J. Climatol. 35 (1), 97–113.
Hwang, T., Band, L.E., Miniat, C.F., Song, C., Bolstad, P.V., Vose, J.M., Love, J.P., 2014. Divergent phenological response to hydroclimate variability in forested mountain watersheds. Glob. Change Biol. 20 (8), 2580–2595.
Irvine, P.J., et al., 2017. Towards a comprehensive climate impacts assessment of solar geoengineering. Earth's Future 5 (1), 93–106.
Jaeger, K.L., Olden, J.D., Pelland, N.A., 2014. Climate change poised to threaten hydrologic connectivity and endemic fishes in dryland streams. Proc. Natl. Acad. Sci. 111 (38), 13894–13899.
Jamieson, P.D., Semenov, M.A., Brooking, I.R., Francis, G.S., 1998. Sirius: a mechanistic model of wheat response to environmental variation. Eur. J. Agron. 8 (3–4), 161–179.
Jasechko, S., Sharp, Z.D., Gibson, J.J., Birks, J.S., Yi, Y., Fawcett, P.J., 2013. Terrestrial water fluxes dominated by transpiration. Nature 496 (7445), 347.
Jolly, W.M., Nemani, R., Running, S.W., 2005. A generalized, bioclimatic index to predict foliar phenology in response to climate. Glob. Change Biol. 11 (4), 619–632.
Kharin, V.V., Zwiers, F.W., Zhang, X., Wehner, M., 2013. Changes in temperature and precipitation extremes in the CMIP5 ensemble. Clim. Change 119 (2), 345–357.
Koetz, B., Baret, F., Poilvé, H., Hill, J., 2005. Use of coupled canopy structure dynamic and radiative transfer models to estimate biophysical canopy characteristics. Remote Sens. Environ. 95 (1), 115–124.
Labat, D., Goddéris, Y., Probst, J.L., Guyot, J.L., 2004. Evidence for global runoff increase related to climate warming. Adv. Water Resour. 27 (6), 631–642.
Leipprand, A., Gerten, D., 2006. Global effects of doubled atmospheric CO_2 content on evapotranspiration, soil moisture and runoff under potential natural vegetation. Hydrol. Sci. J. 51 (1), 171–185.
Lemordant, L., Gentine, P., Stéfanon, M., Drobinski, P., Fatichi, S., 2016. Modification of land atmosphere interactions by CO_2 effects: implications for summer dryness and heat wave amplitude. Geophys. Res. Lett. 43 (19).
Lemordant, L., Gentine, P., Swann, A.S., Cook, B.I., Scheff, J., 2018. Critical impact of vegetation physiology on the continental hydrologic cycle in response to increasing CO_2. Proc. Natl. Acad. Sci. 115 (16), 201720712.
Lian, X., et al., 2018. Partitioning global land evapotranspiration using CMIP5 models constrained by observations. Nat. Clim. Change 8 (7), 640–646.
Matthews, T.K.R., Wilby, R.L., Murphy, C., 2017. Communicating the deadly consequences of global warming for human heat stress. Proc. Natl. Acad. Sci. 114 (15), 3861–3866.
McVicar, T.R., Niel, T.G., Li, L., Hutchinson, M.F., Mu, X., Liu, Z., 2007. Spatially distributing monthly reference evapotranspiration and pan evaporation considering topographic influences. J. Hydrol. 338 (3–4), 196–220.
McVicar, T.R., et al., 2012. Global review and synthesis of trends in observed terrestrial near-surface wind speeds: implications for evaporation. J. Hydrol. 416, 182–205.
Mercado, L.M., Bellouin, N., Sitch, S., Boucher, O., Huntingford, C., Wild, M., Cox, P.M., 2009. Impact of changes in diffuse radiation on the global land carbon sink. Nature 458 (7241), 1014–1017.
Miller, P., Lanier, W., Brandt, S., 2001. Using Growing Degree Days to Predict Plant Stages. Ag/Extension Communications Coordinator, Communications Services, Montana State University-Bozeman, Bozeman, MO.
Monsi, M., Saeki, T., 1953. über den Lichtfaktor in den Pflanzengesellschaften und seine Bedeutung für die Stoffproduktion. Japanese J. Bot. 14, 22–52.
Myneni, R.B., Ramakrishna, R., Nemani, R., Running, S.W., 1997. Estimation of global leaf area index and absorbed par using radiative transfer models. Geosci. Remote Sens. IEEE Trans. 35 (6), 1380–1393.
Nemani, R.R., Keeling, C.D., Hashimoto, H., Jolly, W.M., Piper, S.C., Tucker, C.J., Myneni, R.B., Running, S.W., 2003. Climate-driven increases in global terrestrial net primary production from 1982 to 1999. Science (New York, N.Y.) 300 (5625), 1560–1563.
Orlandi, F., Garcia-Mozo, H., Dhiab, B.A., Galán, C., Msallem, M., Romano, B., Abichou, M., Dominguez-Vilches, E., Fornaciari, M., 2013. Climatic indices in the interpretation of the phenological phases of the olive in mediterranean areas during its biological cycle. Clim. Change 116 (2), 263–284.
Parton, W.J., Logan, J.A., 1981. A model for diurnal variation in soil and air temperature. Agric. Meteorol. 23, 205–216.
Piao, S., Friedlingstein, P., Ciais, P., de Noblet-Ducoudré, N., Labat, D., Zaehle, S., 2007. Changes in climate and land use have a larger direct impact than rising CO_2 on global river runoff trends. Proc. Natl. Acad. Sci. 104 (39), 15242–15247.
Pierret, A., Lacombe, G., 2018. Hydrologic regulation of plant rooting depth: breakthrough or observational conundrum? Proc. Natl. Acad. Sci. 115 (12), 201801721.
Pongratz, J., Lobell, D.B., Cao, L., Caldeira, K., 2012. Crop yields in a geoengineered climate. Nat. Clim. Change 2, 101–105.
Pu, B., Dickinson, R.E., 2012. Examining vegetation feedbacks on global warming in the Community Earth System Model. J. Geophys. Res.: Atmospheres (1984–2012) 117 (D20).
Qi, W., Zhang, C., Fu, G., Zhou, H., 2015. Global Land Data Assimilation System data assessment using a distributed biosphere hydrological model. J. Hydrol. 528, 652–667.
Qi, W., Zhang, C., Fu, G., Sweetapple, C., Zhou, H., 2016a. Evaluation of global fine-resolution precipitation products and their uncertainty quantification in ensemble discharge simulations. Hydrol. Earth Syst. Sci. 20 (2), 903–920.
Qi, W., Zhang, C., Fu, G., Zhou, H., 2016b. Quantifying dynamic sensitivity of optimization algorithm parameters to improve hydrological model calibration. J. Hydrol. 533, 213–223.
Qi, W., Zhang, C., Fu, G., Zhou, H., 2016c. Imprecise probabilistic estimation of design floods with epistemic uncertainties. Water Resour. Res. 52 (6), 4823–4844.
Qi, W., Zhang, C., Fu, G., Zhou, H., Liu, J., 2016d. Quantifying uncertainties in extreme flood predictions under climate change for a medium-sized basin in northeast China. J. Hydrometeorol. 17, 3099–3112.
Qi, W., Liu, J., Chen, D., 2018a. Evaluations and improvements of GLDAS2.0 and GLDAS2.1 forcing data's applicability for basin scale hydrological simulations in the Tibetan Plateau. J. Geophys. Res.: Atmospheres 123.
Qi, W., Liu, J., Yang, H., Sweetapple, C., 2018b. An ensemble-based dynamic Bayesian averaging approach for discharge simulations using multiple global precipitation products and hydrological models. J. Hydrol. 558, 405–420.
Qi, W., Zhang, C., Fu, G., Sweetapple, C., Liu, Y., 2018c. Impact of robustness of hydrological model parameters on flood prediction uncertainty. J. Flood Risk Manage., e12488.
Rabus, B., Eineder, M., Roth, A., Bamler, R., 2003. The shuttle radar topography mission—a new class of digital elevation models acquired by spaceborne radar. ISPRS J. Photogramm. Remote Sens. 57 (4), 241–262.
Ramirez, J.A., Finnerty, B., 1996. CO_2 and temperature effects on evapotranspiration and irrigated agriculture. Agron. J. 122, 155–163.
Randall, D.A., et al., 1996. A revised land surface parameterization (SiB2) for GCMS. Part III: the greening of the Colorado state university general circulation model. J. Clim. 9 (4), 738–763.
Rehana, S., Mujumdar, P.P., 2011. River water quality response under hypothetical climate change scenarios in Tunga Bhadra River, India. Hydrol. Processes 25 (22), 3373–3386.
Reich, P.B., Hobbie, S.E., Lee, T.D., 2014. Plant growth enhancement by elevated CO_2 eliminated by joint water and nitrogen limitation. Nat. Geosci. 7 (12), 920–924.
Savoy, P., Mackay, S.D., 2015. Modeling the seasonal dynamics of leaf area index based on environmental constraints to canopy development. Agric. For. Meteorol. 200, 46–56.

Sawada, Y., Koike, T., Jaranilla-Sanchez, P.A., 2014. Modeling hydrologic and ecologic responses using a new eco-hydrological model for identification of droughts. Water Resour. Res. 50 (7), 6214–6235.
Schymanski, S.J., Or, D., 2016. Wind increases leaf water use efficiency. Plant Cell Environ. 39 (7), 1448–1459.
Seager, R., et al., 2007. Model projections of an imminent transition to a more arid climate in southwestern North America. Science 316 (5828), 1181–1184.
Sellers, P.J., Randall, D.A., Collatz, G.J., Berry, J.A., Field, C.B., Dazlich, D.A., Zhang, C., Collelo, G.D., Bounoua, L., 1996a. A revised land surface parameterization (SiB2) for atmospheric GCMS. Part I: model formulation. J. Clim. 9 (4), 676–705.
Sellers, P.J., Tucker, C.J., Collatz, G.J., Los, S.O., Justice, C.O., Dazlich, D.A., Randall, D.A., 1996b. A revised land surface parameterization (SiB2) for atmospheric GCMS. Part II: the generation of global fields of terrestrial biophysical parameters from satellite data. J. Clim. 9 (4), 706–737.
Seneviratne, S.I., Donat, M.G., Pitman, A.J., Knutti, R., Wilby, R.L., 2016. Allowable CO_2 emissions based on regional and impact-related climate targets. Nature 529 (7587), 477–483.
Seneviratne, S.I., et al., 2018. Land radiative management as contributor to regional-scale climate adaptation and mitigation. Nat. Geosci. 11 (2), 88–96.
Setiyono, T.D., Weiss, A., Specht, J.E., Cassman, K.G., Dobermann, A., 2008. Leaf area index simulation in soybean grown under near-optimal conditions. Field Crops Res. 108 (1), 82–92.
Shiogama, H., Stone, D., Emori, S., Takahashi, K., Mori, S., Maeda, A., Ishizaki, Y., Allen, M.R., 2016. Predicting future uncertainty constraints on global warming projections. Sci. Rep. 6, 18903.
Sitch, S., et al., 2003. Evaluation of ecosystem dynamics, plant geography and terrestrial carbon cycling in the LPJ dynamic global vegetation model. Glob. Change Biol. 9 (2), 161–185.
Skinner, C.B., Poulsen, C.J., Mankin, J.S., 2018. Amplification of heat extremes by plant CO_2 physiological forcing. Nat. Commun. 9 (1), 1094.
Steinschneider, S., Polebitski, A., Brown, C., Letcher, B.H., 2012. Toward a statistical framework to quantify the uncertainties of hydrologic response under climate change. Water Resour. Res. 48 (11), W11525.
Stern, N., 2006. Stern Review: The Economics of Climate Change. HM Treasury, London.
Streck, N.A., 2005. Climate change and agroecosystems: the effect of elevated atmospheric CO_2 and temperature on crop growth, development, and yield. Ciência Rural 35 (3), 730–740.
Su, L., Wang, Q., Wang, C., Shan, Y., 2015. Simulation models of leaf area index and yield for cotton grown with different soil conditioners. PLoS One 10 (11).
Swann, A.L.S., Hoffman, F.M., Koven, C.D., Randerson, J.T., 2016. Plant responses to increasing CO_2 reduce estimates of climate impacts on drought severity. Proc. Natl. Acad. Sci. 113 (36), 10019–10024.
Tao, B., Tian, H., Ren, W., Yang, J., Yang, Q., He, R., Cai, W., Lohrenz, S., 2014. Increasing Mississippi river discharge throughout the 21st century influenced by changes in climate, land use, and atmospheric CO_2. Geophys. Res. Lett. 41 (14), 4978–4986.
Tesemma, Z.K., Wei, Y., Peel, M.C., Western, A.W., 2015. Including the dynamic relationship between climatic variables and leaf area index in a hydrological model to improve streamflow prediction under a changing climate. Hydrol. Earth Syst. Sci. 19 (6), 2821–2836.
Tolson, B.A., Shoemaker, C.A., 2007. Dynamically dimensioned search algorithm for computationally efficient watershed model calibration. Water Resour. Res. 43 (1), W01413.
Tolson, B.A., Shoemaker, C.A., 2008a. Reply to comment on "Dynamically dimensioned search algorithm for computationally efficient watershed model calibration" by Ali Behrangi. Water Resour. Res. 44 (12).
Tolson, B.A., Shoemaker, C.A., 2008b. Efficient prediction uncertainty approximation in the calibration of environmental simulation models. Water Resour. Res. 44 (4), W04411.
Tolson, B.A., Asadzadeh, M., Maier, H.R., Zecchin, A., 2009. Hybrid discrete dynamically dimensioned search (HD-DDS) algorithm for water distribution system design optimization. Water Resour. Res. 45 (12), W12416.
Trancoso, R., Larsen, J.R., McVicar, T.R., Phinn, S.R., McAlpine, C.A., 2017. CO_2-vegetation feedbacks and other climate changes implicated in reducing base flow. Geophys. Res. Lett. 44 (5), 2310–2318.
Walling, B., Chaudhary, S., Dhanya, C.T., Kumar, A., Walling, B., Chaudhary, S., Dhanya, C.T., Kumar, A., 2017. Estimation of environmental flow incorporating water quality and hypothetical climate change scenarios. Environ. Monit. Assess. 189 (5), 225.
Wang-Erlandsson, L., van der Ent, R.J., Gordon, L.J., Savenije, H.H.G., 2014. Contrasting roles of interception and transpiration in the hydrological cycle – part 1: temporal characteristics over land. Earth Syst. Dyn. 5 (2), 441–469.
Wang, F., Wang, L., Koike, T., Zhou, H., Yang, K., Wang, A., Li, W., 2011. Evaluation and application of a fine-resolution global data set in a semiarid mesoscale river basin with a distributed biosphere hydrological model. J. Geophys. Res.: Atmospheres 116 (D21).
Wang, L., Koike, T., Yang, K., Jackson, T.J., Bindlish, R., Yang, D., 2009. Development of a distributed biosphere hydrological model and its evaluation with the Southern Great Plains Experiments (SGP97 and SGP99). J. Geophys. Res.: Atmospheres 114 (D8).
Wilby, R.L., Harris, I., 2006. A framework for assessing uncertainties in climate change impacts: low-flow scenarios for the River Thames, UK. Water Resour. Res. 42 (2), W02419.
Wild, M., et al., 2005. From dimming to brightening: decadal changes in solar radiation at Earth's surface. Science 308 (5723), 847–850.
Wild, M., 2009. Global dimming and brightening: a review. J. Geophys. Res.: Atmospheres (1984–2012) 114 (D10).
Willett, K.M., Jones, P.D., Gillett, N.P., Thorne, P.W., 2008. Recent changes in surface humidity: development of the HadCRUH dataset. J. Clim. 21 (20), 5364–5383.
Wu, Y., Liu, S., Abdul-Aziz, O.I., 2012a. Hydrological effects of the increased CO_2 and climate change in the Upper Mississippi River Basin using a modified SWAT. Clim. Change 110 (3–4), 977–1003.
Wu, Y., Liu, S., Gallant, A.L., 2012b. Predicting impacts of increased CO_2 and climate change on the water cycle and water quality in the semiarid James River Basin of the Midwestern USA. Sci. Total Environ. 430, 150–160.
Yang, K., Koike, T., Ye, B., 2006. Improving estimation of hourly, daily, and monthly solar radiation by importing global data sets. Agric. For. Meteorol. 137 (1–2), 43–55.
Yang, Y., Donohue, R.J., McVicar, T.R., Roderick, M.L., Beck, H.E., 2016. Long-term CO_2 fertilization increases vegetation productivity and has little effect on hydrological partitioning in tropical rainforests. J. Geophys. Res. Biogeosci. 121 (8), 2125–2140.
Yao, Y., et al., 2018. Spatiotemporal pattern of gross primary productivity and its covariation with climate in China over the last thirty years. Glob. Change Biol. 24 (1), 184–196.
Zhang, Y., et al., 2016. Multi-decadal trends in global terrestrial evapotranspiration and its components. Sci. Rep. 6 (1), 19124.
Zhu, Z., et al., 2016. Greening of the Earth and its drivers. Nat. Clim. Change 6 (8), 791–795.